Clathrin-mediated Endocytosis Facilitates Internalization of *Magnaporthe oryzae* Effectors into Rice Cells

Ely Oliveira-Garcia[1,2]*, Tej Man Tamang[1,3], Jungeun Park[3], Melinda Dalby[1], Magdalena Martin-Urdiroz[4], Clara Rodriguez Herrero[4,5], An Hong Vu[2], Sunghun Park[3], Nicholas J. Talbot[5] & Barbara Valent[1]*

[1]Department of Plant Pathology, Kansas State University, Manhattan, KS 66506, U.S.A.

[2]Department of Plant Pathology and Crop Physiology, Louisiana State University Agricultural Center, Baton Rouge, LA 70803, U.S.A.

[3]Department of Horticulture and Natural Resources, Kansas State University, Manhattan, KS 66506, U.S.A.

[4]School of Biosciences, University of Exeter, Exeter, EX4 4QD, UK

[5]The Sainsbury Laboratory, Norwich Research Park, Norwich NR4 7UH, UK.

*Corresponding authors: E. Oliveira-Garcia; E-mail: EOliveiraGarcia@agcenter.lsu.edu and B. Valent; E-mail: bvalent@ksu.edu

Short Title: Blast Effector Translocation By Plant Endocytosis

* The author(s) responsible for distribution of materials integral to the findings presented in this article in accordance with the policy described in the Instructions for Authors (https://academic.oup.com/plcell/pages/General-Instructions) are: E. Oliveira-Garcia (EOliveiraGarcia@agcenter.lsu.edu) and B. Valent (bvalent@ksu.edu).

ABSTRACT

Many filamentous eukaryotic plant pathogens, such as fungi and oomycetes, deliver effectors into living plant cells to suppress defenses and control plant processes needed for infection. Little is known about the mechanism by which these pathogens translocate effector proteins across the plasma membrane into the plant cytoplasm. The blast fungus *Magnaporthe oryzae* secretes cytoplasmic effectors into a specialized biotrophic interfacial complex (BIC) before translocation. Here we show that cytoplasmic effectors within BICs are packaged into dynamic vesicles that can occasionally be found separated from BICs in the host cytoplasm. Live cell imaging with fluorescently-labelled rice lines showed that BICs are enriched in plant plasma membrane, actin, and Clathrin Light Chain-1, a marker for clathrin-mediated endocytosis (CME). We report that a novel cytoplasmic effector, Bas83, labels empty membrane vesicles surrounding BICs. Inhibition of CME using VIGS and chemical treatments results in a distinctive swollen BIC phenotype lacking effector vesicles. In contrast, fluorescent marker co-localization, VIGS and chemical inhibitor studies failed to support a major role for clathrin-independent endocytosis in effector vesicle formation. Taken together, this study provides evidence that cytoplasmic effector translocation is mediated by clathrin-mediated endocytosis in BICs and suggests a role for *M. oryzae* effectors in co-opting plant endocytosis.

INTRODUCTION

Many fungal and oomycete pathogens cause plant disease by hijacking and feeding on living plant cells, and they deliver effectors into and around host cells to promote infection (Giraldo and Valent, 2013; Lo Presti and Kahmann, 2017). This includes the Ascomycete fungus *Magnaporthe oryzae* (synonym of *Pyricularia oryzae*), which threatens global food security by causing blast diseases on rice, on several millets, and most recently on wheat (Gladieux et al., 2018; Valent et al., 2020). *M. oryzae* executes a hemibiotrophic lifestyle involving biotrophic invasion of successive plant cells by specialized intracellular invasive hyphae (IH) that grow from cell to cell (Kankanala et al., 2007). Blast IH growing in living host cells are enclosed by extensions of the plant plasma membrane termed the extra-invasive hyphal membrane (EIHM). Colonized cells die as they fill with hyphae and the EIHM and host vacuolar membranes become disrupted, while the fungus moves on to colonize neighboring cells using the same strategy (Kankanala et al., 2007; Mochizuki et al., 2015; Sakulkoo et al., 2018; Jones et al., 2021). Each successful IH undergoes

56 hyphal morphogenesis and is associated with differentiated interfacial zones after entering the host
57 cell lumen (Kankanala et al., 2007; Khang et al., 2010). Specifically, appressorial penetration pegs
58 enlarge into tubular filamentous hyphae, called primary invasive hyphae, which are enclosed in
59 EIHM with an extended dome-shaped cap, the Biotrophic Interfacial Complex (BIC). BICs
60 accumulate cytoplasmic effectors destined for translocation into the host cytoplasm. Tubular
61 primary hyphae then transition to a bulbous pseudohyphal-like growth form. BICs at the tips of
62 primary hyphae are left behind beside the first bulbous IH cell during the differentiation process,
63 and they continue to accumulate cytoplasmic effectors as the bulbous IH grow to fill the cell
64 (Khang et al., 2010). Mutation in an effector gene, Required-for-Focal-BIC-Formation 1 (*RBF1*),
65 encoding a glycine-rich secreted protein, results in dispersed cytoplasmic effector localization
66 around BIC-associated cells (the primary hyphae and first bulbous IH cell), perturbs primary
67 hyphal structure, and decreases pathogenicity (Nishimura et al., 2016; Nishizawa et al., 2016).
68 In blast disease, cytoplasmic and apoplastic effectors are clearly differentiated by the
69 fungal secretion system used and their localization pattern after secretion. Primary hyphae and the
70 first bulbous IH focally secrete cytoplasmic effectors into BICs using a specialized, Golgi-
71 independent secretion system. In *M. oryzae*, and also in the oomycete potato pathogen
72 *Phytophthora infestans*, secretion of cytoplasmic effectors differs from secretion of apoplastic
73 effectors in being insensitive to treatment with Brefeldin A (BFA), a chemical known to inhibit
74 conventional Golgi-mediated secretion in fungi (Giraldo et al., 2013; Van den Ackerveken, 2017;
75 Wang et al., 2017). Fluorescent cytoplasmic effectors are routinely detected in the cytoplasm of
76 invaded cells, and some are also detected in the cytoplasm of surrounding uninvaded host cells,
77 apparently moving through plasmodesmata to prepare neighboring cells before invasion (Khang
78 et al., 2010). In contrast, apoplastic effectors, such as the biotrophy-associated secreted protein 4
79 (Bas4), the LysM protein 1 (Slp1), and Bas113, are secreted via conventional golgi-mediated
80 secretion, and they accumulate uniformly throughout the apoplastic compartment enclosed within
81 the EIHM, outlining the entire IH without bleeding into the plant cell wall (Mosquera et al., 2009;
82 Mentlak et al., 2012; Giraldo et al., 2013). Indeed, localization of secreted Bas4 fluorescent fusion
83 proteins has become a reliable live cell imaging marker for the intactness of the EIHM around IH
84 (Khang et al., 2010; Mochizuki et al., 2015; Jones et al., 2021). After filling the host cell, hyphal
85 differentiation and BIC relocalization recur for each new hypha that enters a living neighbor cell
86 (Khang et al., 2010; Sakulkoo et al., 2018).

87 The mechanism by which eukaryotic filamentous plant pathogens deliver effectors across
88 the host plasma membrane inside living host cells is poorly understood and the mechanism is likely
89 to vary in different systems (Giraldo and Valent, 2013; Petre and Kamoun, 2014; Fawke et al.,
90 2015; Lo Presti et al., 2015; Lo Presti and Kahmann, 2017). Amino acid translocation motifs have
91 been identified for oomycete effectors, with the RXLR motif being the most common, although
92 cell entry motifs for fungal effectors have not been defined. The RXLR motif in oomycete effectors
93 was reported to mediate host cell uptake through endocytosis based on binding to
94 phosphatidylinositol-3-phosphate (PI3P) in host membrane (Kale et al., 2010), although it was
95 recently shown that the RXLR motif from *Phytophthora infestans* effector AVR3a is cleaved off
96 before secretion from the pathogen (Wawra et al., 2017). Therefore, the function of RXLR motif
97 in cell entry remains disputed (Petre and Kamoun, 2014; Trusch et al., 2018). Another amino acid
98 motif, YKARK, appears involved in translocation of the effector SpHtp3 from *Saprolegnia*
99 *parasitica*, a serious oomycete pathogen of fish, inside fish cells (Trusch et al., 2018). Specifically,
100 this effector appears to be internalized inside host cells via lipid-raft mediated endocytosis through
101 binding to a gp96-like receptor, and another effector is involved in releasing SpHtp3 from vesicles
102 into the fish cytoplasm. In an example from a fungal pathogen, a solvent-exposed RGD
103 vitronectin-like motif is required for internalization of ToxA, a host-specific proteinaceous toxin
104 secreted by the necrotrophic wheat pathogen *Pyrenophora tritici-repentis* (Manning and Ciuffetti,
105 2005). In addition to uptake by plant endocytosis, effectors might enter plant cells through
106 specialized translocon complexes in the plasma membrane. For example, the human malaria
107 parasite, *Plasmodium falciparum*, is contained within a parasitophorous vacuole inside invaded
108 red blood cells, and effectors are delivered across the membrane into the host cytoplasm by the
109 PTEX translocon (Elsworth et al., 2014). Recently, a stable protein complex comprised of five
110 unrelated fungal effectors and two fungal membrane proteins has been implicated in effector
111 translocation by the maize smut fungus *Ustilago maydis* (Ludwig et al., 2021). However, the
112 question of how effectors are taken up into plant cells remains largely unresolved for eukaryotic
113 plant pathogens.
114 Clathrin-mediated endocytosis (CME) is the major mechanism by which eukaryotic cells
115 internalize extracellular or membrane-bound cargoes, and this process is best understood in
116 mammalian systems and yeast (Kaksonen and Roux, 2018). Increasing understanding of CME in
117 plants shows both conserved and evolutionarily unique mechanistic details (Qi et al., 2018;

118 Reynolds et al., 2018; Johnson et al., 2020; Narasimhan et al., 2020). CME is known to play key
119 roles in plant-microbe interactions (Dodds and Rathjen, 2010; Beck et al., 2012; Fan et al., 2015).
120 CME is required for immunity mediated by pattern recognition receptor kinases, for instance,
121 specifically through internalization of activated extracellular pattern recognition receptors (PRRs)
122 for degradation in the vacuole (Mbengue et al., 2016). Examples include the pattern recognition
123 receptor Pep receptor 1/2 (PEPR1/2), the EF-TU receptor (EFR) recognizing the PAMP bacterial
124 elongation factor, and FLS2 recognizing the PAMP flagellin (flg-22) (Spallek et al., 2013;
125 Mbengue et al., 2016), as well as the Cf-4 receptor-like protein that recognizes the *C. fulvum* Avr4
126 avirulence effector (Postma et al., 2016). Trafficking of activated PRRs requires clathrin and
127 converges onto endosomal vesicles that are also shared by the hormone receptor Brassinosteriod
128 Insensitive 1 (BRI1). Additionally, it is known that pathogens can control plant CME. In addition
129 to its role in suppressing INF1-mediated cell death, the *P. infestans* host-translocated RXLR
130 effector AVR3a was recently shown to associate with the Dynamin-Related Protein 2, a plant
131 GTPase implicated in receptor-mediated endocytosis, and to suppress flg22-triggered defense
132 responses and reduce FLS2 internalization (Chaparro-Garcia et al., 2015). Therefore, AVR3a
133 interacts with a membrane-remodeling complex involved in immune receptor-mediated
134 endocytosis. Also, in host cells containing haustoria from the oomycete *P. infestans*, the late
135 endosomal pathway is rerouted from the vacuole to the extrahaustorial membrane (EHM)
136 surrounding haustoria (Bozkurt et al., 2015). Multiple effectors from this pathogen are now
137 implicated in rerouting the host membrane trafficking system and autophagy machinery for the
138 benefit of the invading pathogen (Bozkurt et al., 2015; Dagdas et al., 2018; Petre et al., 2021).
139 Effector translocation in the *M. oryzae*/rice pathosystem can be assayed directly by live
140 cell imaging of fluorescently-labeled effector proteins inside host cells after secretion by IH
141 invading rice leaf sheath cells (Khang et al., 2010). Although some effectors naturally localize to
142 host nuclei, addition of a nuclear localization signal (NLS) to fluorescent effectors enhances
143 visualization of translocation and cell-to-cell movement. Blast cytoplasmic effectors apparently
144 do not contain a translocation motif as reported for oomycete effectors. Instead, preferential
145 accumulation in the BIC, which is a prominent feature of the *M. oryzae*-rice cell interface, is the
146 major predictor for translocation into the rice cell. Previously, Nishizawa and colleagues reported
147 that a cytoplasmic effector occurs in vesicles in an outer BIC region (Mochizuki et al., 2015;
148 Nishimura et al., 2016; Nishizawa et al., 2016). Here, we have used live-cell fluorescence imaging

149 to characterize the nature and dynamics of membrane-bound effector vesicles within BICs and in
150 surrounding host cytoplasm. We show that BICs are enriched for CME components, and we report
151 functional analyses using virus-induced gene silencing (VIGS) and pharmacological approaches.
152 When considered together, our data indicate that blast effectors are internalized through clathrin-
153 mediated endocytosis in the outer BIC layers, followed by escape from the vesicles into the rice
154 cytoplasm.
155

156 **RESULTS**
157

158 **BICs contain multiple vesicles labeled by cytoplasmic effectors**

159 BICs were previously reported as interfacial structures containing fluorescently-labelled
160 apoplastic effectors, such as Bas4:eGFP, in an inner base layer and a concentration of fluorescent
161 cytoplasmic effectors in the outer 'dome-shaped' region (Khang et al., 2010; Nishizawa et al.,
162 2016). We now routinely resolve the dome region of BICs by laser confocal imaging as a
163 concentration of vesicles containing fluorescent cytoplasmic effectors (Figure 1). These effector
164 vesicles are illustrated by an image of a BIC at the tip of a primary hypha (tip-BIC) expressing
165 fluorescent apoplastic effector Bas4:eGFP and fluorescent cytoplasmic effector Pwl2:mRFP
166 (Figure 1A). The Bas4:eGFP fluorescence remains evenly distributed throughout the EIHM matrix
167 around the growing IH, including in an inner layer of the BIC. In contrast, Pwl2:mRFP occurs as
168 distinct vesicles in the outer BIC region. We have observed effector vesicles in tip-BICs labeled
169 with additional translocated effectors Bas1 and Pwl1 fused to either eGFP or mRFP (Supplemental
170 Figure S1). Vesicles are also observed after tip-BICs move beside the first bulbous IH cells (side-
171 BICs) (Figure 1B; Figure S2). We evaluated the proximity of these vesicles relative to both tip-
172 and side-BICs. Whereas the vast majority of vesicles associated with primary IH were located in
173 the tip-BIC, some vesicles associated with side-BICs were found in regions of the cytoplasm at
174 least 7 µm from the fungal cell wall at the BIC, which we define as outside the BIC (Figure 1C).
175 Inclusion of the apoplastic effector Bas4:eGFP in these experiments confirmed that the EIHM
176 remained intact at each infection site, based on its uniform outlining of the IH and lack of spilling
177 into the invaded rice cell.

178 We identified a novel cytoplasmic effector, Bas170 (MGG_07348.6), that localized in
179 vesicles in the rice cytoplasm short distances from the appressorial penetration site at a stage before
180 primary hyphal growth is visible. The Bas170:mRFP fusion protein naturally accumulates in the

181 rice nucleus at this very early infection stage, presumably to reprogram plant transcription essential
182 for *M. oryzae* infection (Figure 1D). These results suggest rapid effector translocation from
183 appressoria even before growth of primary IH. Bas170:mRFP also labels BIC-associated vesicles
184 in tip-BICs and side BICs after growth of IH in the cell (Figure 1E,F). Vesicles observed using
185 fluorescent Bas170 fusion proteins are similar to vesicles observed with Pwl2, Pwl1 and Bas1
186 fusion proteins except that these latter effectors were not observed under appressoria at the earlier
187 time period.

188 **Vesicles in BICs are dynamic through time**

189 To understand vesicle dynamics in BICs through time, we imaged BIC effector fluorescence
190 during the morphogenic switch from tubular primary hyphae to bulbous IH using a strain co-
191 expressing two cytoplasmic effectors, Bas1:eYFP and Pwl2:mRFP (Figure 2). The vesicle content
192 varied over the 2-hour period when the tip-BIC was displaced from the primary hyphal tip to the
193 side-BIC beside the differentiating bulbous IH cell. Tip-BICs often contained vesicles with either
194 red or green fluorescence, rather than yellow expected for co-localization, suggesting that effectors
195 can be sorted into different vesicles. For this series of experiments, Pwl2:mRFP occurred in
196 vesicles that reached outer layers of the tip-BIC compared to Bas1:eYFP. Pwl2:mRFP appeared
197 less abundant relative to Bas1:eYFP during the switch from tip- to side-BIC, recovering again after
198 growth of bulbous IH (Figure 2A). Both vesicle size and content vary within BICs through time
199 (Figure 2 B-F). Specifically, BICs at primary hyphal tips contain a larger number of smaller
200 vesicles (Figure 2D,E). Whereas BICs on primary hyphae deliver effectors in 'micro-vesicles'
201 ranging from 41 nm to 114 nm, BICs on mature bulbous hypha contain effectors in 'macro-
202 vesicles' ranging from 153 nm up to 2310 nm at times (Figure 2C,D). Effector vesicles beside
203 mature bulbous IH often showed colocalization of fluorescence from different effectors compared
204 to vesicles in tip-BICs (Figure 2A, B and F).

205 Cytoplasmic connections were observed between BICs and plant cytoplasm at the
206 periphery of the invaded cell, illustrated in optical sections through a BIC in Supplemental Movie
207 S1. This is consistent with a previous report of dynamic connections linking BICs and host
208 cytoplasm underneath the appressorium (Khang et al., 2010). These cytoplasmic connections may
209 facilitate movement of effectors from cytoplasm surrounding the BIC in the cell center to the
210 peripheral cytoplasm, in position to rapidly move through plasmodesmata into neighboring cells.

211 **BIC vesicles contain plant plasma membrane**

212 Effector-labeled vesicles in the BIC could arise through secretion of cytoplasmic effectors in
213 fungal exosomes or through plant endocytosis. We previously reported that BICs are enriched in
214 plant plasma membrane based on infection of transgenic rice expressing a plasma membrane
215 marker (Giraldo et al., 2013). Here we again use LTi6B:GFP-labeled rice to confirm that BICs
216 contain abundant plant plasma membrane (Figure 3A,B). Individual effector vesicles were
217 observed to be surrounded by labeled plant plasma membrane (Figure 3C), especially for vesicles
218 in side-BICs on mature bulbous hyphae, where the vesicles reach diameters of 150 nm or larger.

219 To further confirm that BIC vesicles contain plant plasma membrane, we evaluated BIC
220 membrane composition by staining with the endocytosis tracker dyes FM 4-64 and FM 1-4 (Figure
221 3D,E). These amphiphilic styryl dyes insert in the plasma membrane where they diffuse laterally
222 in the membrane and are only internalized into the cell via endocytosis (Atkinson et al., 2002;
223 Bolte et al., 2004). We previously showed that FM 4-64 is prevented from inserting in IH
224 membranes, which are sealed inside the EIHM (Kankanala et al., 2007). Exclusion of these dyes
225 from fungal membranes was documented by the lack of fluorescent labeling of the fungal septa
226 and vacuoles, which occurs if the dye inserts in the fungal plasma membrane (Atkinson et al.,
227 2002; Kankanala et al., 2007). Infected rice cells treated with FM 4-64 and FM 1-43 showed
228 massive accumulation of these dyes in both tip- and side-BICs (Figure 3D). Images of BICs stained
229 with FM 4-64 showed vesicles carrying effectors immersed in the region of intense staining
230 associated with the BICs (Figure 3E). Vesicles that carry effectors were also observed separated
231 from the BIC, presumably in the rice cytoplasm (Figure 3E, inset upper right), but effector-
232 containing vesicles have not been frequently observed at long distances from the BIC
233 (Supplemental Movie S2). Apparent vesicular bursting was also observed, which suggests that the
234 vesicles are unstable, presumably releasing the effector contents into the host cytoplasm. Taken
235 together, these results indicate that BIC-associated effector vesicles are more likely derived
236 through plant endocytosis than from secretion of fungal exosomes.

237 **Bas83 is a unique cytoplasmic effector that associates with rice membrane concentrating**
238 **around BICs**

239 Since it is likely that specific blast effectors play roles in vesicle formation and effector
240 translocation, we were particularly interested in effectors that appear to associate with membranes
241 in host cells. The *BAS83* (MGG_08506.6) gene is unique to *M. oryzae*, and it is 36-fold upregulated

242 during biotrophic invasion (Mosquera et al., 2009). Bas83:mRFP is translocated into invaded host
243 cells, but it does not precisely colocalize with other BIC-localized cytoplasmic effectors
244 Pwl2:eGFP and Pwl1:eGFP (Figure 4A; Supplemental Figure S3). In contrast, Bas83:mRFP seems
245 to label the EIHM surrounding the BIC-associated cells, the primary hyphae and first bulbous IH,
246 and it labels membrane bubbles, or vesicles, near to BICs and BIC-associated cells (Figure 4A-C).
247 Figure 4A shows that Bas83:mRFP-labeled vesicles do not contain the cytoplasmic effector
248 Pwl2:eGFP, indicating they are distinct from effector vesicles in BICs. Bas83:mRFP is also
249 associated with vesicles observed under appressoria (Figure 4C; Supplemental Figure S3).
250 However, Bas83:mRFP fails to label membrane surrounding subsequently formed bulbous IH that
251 are associated with apoplastic effectors and not with cytoplasmic effectors (see 2nd bulbous IH in
252 Figure 4C). We hypothesize that Bas83 is involved in recruiting new plant plasma membrane to
253 form the EIHM and BICs during biotrophic development. However, repeated attempts in two
254 different laboratories (264 purified transformants, 4 methods and 5 experiments; KSU and Univ.
255 of Exeter) failed to produce knock-out mutants for further functional analysis (Supplemental
256 Figure S4).

257 **BICs contain plant actin**

258 The actin cytoskeleton is essential for endocytic processes including plasma membrane folding,
259 vesiculation, and vesicle transport (Grassart et al., 2014; Narasimhan et al., 2020). Effector vesicle
260 formation in BICs suggests that this interfacial structure should contain abundant host actin.
261 Therefore, we imaged plant actin dynamics during biotrophic invasion using rice lines expressing
262 the actin marker LifeAct:eGFP. Infection by *M. oryzae* strains expressing chimeric protein
263 Pwl2:mRFP showed massive colocalization of LifeAct:eGFP in BICs (Figure 5A). Actin was
264 abundant in all imaged tip- and side-BICs (Figure 5B). Likewise, colocalization of fluorescent
265 Phalloidin conjugates and fluorescently-labeled effector confirmed that BICs are rich in plant actin
266 filaments (Figure 5C). We hypothesize that actin filaments are responsible for plasma membrane
267 manipulation, vesiculation and possibly for the transport of vesicles carrying effectors into the rice
268 cell cytoplasm.

269 **BICs consistently contain abundant plant clathrin, but not flotillin**

270 Clathrin-mediated endocytosis (CME) is the major endocytosis mechanism in plants, with some
271 contribution by Clathrin-independent endocytosis (CIE) (Chen et al., 2011; Ewers and Helenius,

272 2011; Fan et al., 2015; Narasimhan et al., 2020). To assess co-localization of specific endocytosis
273 markers with BICs, we generated transgenic rice lines expressing a fluorescent marker for either
274 CME or CIE. For CME, we generated a C-terminal translational fusion of eGFP with the rice
275 Clathrin light chain-1 (OsCLC1), which is a component of the clathrin coat together with clathrin
276 heavy chain. Rice lines expressing OsCLC1:eGFP show typical clathrin foci (Konopka et al.,
277 2008; Narasimhan et al., 2020) in uninfected rice cells (Figure 6). The marker for CIE was a C-
278 terminal translational fusion of eGFP to flotillin (Flot1), which is a component of lipid rafts (Otto
279 and Nichols, 2011; Li et al., 2012). Rice lines with the CME and CIE markers were used for leaf
280 sheath assays with an *M. oryzae* strain expressing Pwl2:mRFP to label BICs. In addition to typical
281 clathrin foci around the cell periphery, all tip-BICs and side-BICs contain fluorescence from
282 OsCLC1:eGFP co-localizing with Pwl2:mRFP (Figure 6A and C). Clathrin fluorescence could
283 sometimes be observed co-localizing with effector fluorescence in BIC vesicles (Supplemental
284 Movie S3). In contrast, very few (~4%) tip-BICs colocalized with Flot1:eGFP. Some
285 colocalization of Flot1:eGFP and Pwl2:mRFP occurred in side-BICs besides mature bulbous
286 hyphae (Figure 6B,C). Colocalization results from several independent experiments were
287 consistent with a major role for CME, but not for CIE, in the internalization of cytoplasmic
288 effectors.

289 **Silencing of rice endocytosis machinery blocks *M. oryzae* infection**

290 We assessed the impact of inhibition of CME and CIE on BICs and effector vesicles using the
291 brome mosaic virus system (Ding et al., 2006; Ding et al., 2007) for silencing of genes for CME
292 and CIE components that have been characterized by gene silencing analyses in *Arabidopsis*.
293 Specifically, we silenced two rice CME genes, Adaptor protein complex-2 subunit α2 (*AP-2α*) and
294 clathrin heavy chain-1 (*CHC1*) (Di Rubbo et al., 2013; Larsson et al., 2017) as well as the CIE
295 gene *Flotillin-1* (*Flot1*) (Li et al., 2012). Silencing of both CME components *AP-2α* and *CHC1*
296 resulted in severe reduction in pathogenicity in whole plant spray inoculation assays (Figure
297 7A,B). However, as expected, silencing of these genes caused stunting and decreased plant health
298 (Supplemental Figure S5), and levels of pathogenicity in blast disease are known to be decreased
299 on unhealthy rice plants. More significant is the phenotype of pathogen blockage at individual
300 infection sites. Silencing of either CME component RNAi*AP-2α* or RNAi*CHC1* led to a distinctive
301 swollen BIC phenotype, with enlarged, abnormally-shaped BICs that lack effector vesicles (Figure
302 7C-F). By contrast, silencing of the CIE marker gene *Flot1* showed less severe stunting

303 (Supplemental Figure S5), less of an impact on pathogenicity (Figure 7A,B), and minor impact on
304 BIC structure (Figure 7C-F). For example, compare the 28 hpi images of BICs in control rice
305 plants with the RNAi*Flot1*-silenced and the RNAi*AP-2*α-silenced rice plants in Figure 7C, and
306 quantification of swollen BIC events in Figure 7F.

307 In addition to swollen BICs at sites with primary hyphae, silencing of both CME genes
308 decreased appressorial penetration and induced the accumulation of the cytoplasmic effector
309 Pwl2:mRFP under failed penetration sites where it is not normally observed (Figure 7D,E). In
310 contrast, silencing of *Flot1* had only minor effects on appressorium penetration success and on
311 accumulation of Pwl2:mRFP under failed appressoria. Like our finding of early accumulation of
312 Bas170 under appressoria before penetration, these results again suggest that effector uptake
313 begins before host penetration. These results also suggest that CME plays a role in effector
314 translocation at the appressorial penetration stage as well as from BICs.

315 **Chemical inhibition of rice endocytosis machinery blocks *M. oryzae* infection**

316 Pharmacological approaches have impacted studies in diverse biological systems (Robinson et al.,
317 2008; Hicks and Raikhel, 2010; Grassart et al., 2014; Fan et al., 2015). To further assess potential
318 impact of the plant endocytic machinery on cytoplasmic effector translocation, we tested a series
319 of chemicals that are reported to inhibit plant CME or CIE (Table 1). Compared with the non-
320 treated control (Figure 8A), treatment with reported CME inhibitor cantharidin led to abnormally-
321 shaped swollen BICs that lack distinct effector vesicles, resembling those seen with silencing of
322 CME components (Figure 8B). Fluorescence intensity linescans confirm that cantharidin treatment
323 had little, if any, impact on localization of apoplastic effector Bas4:eGFP in the base of the BIC.

324 Subsequent quantification of cantharidin treatment along with treatment of 2 additional
325 reported CME inhibitors, chlorpromazine and triclosan (Table 1), showed a high proportion of
326 swollen, irregular-shaped cytoplasmic effector fluorescence patterns in BICs (Figure 9A-C). By
327 contrast, inhibition of CIE with filipin and methyl-β-cyclodextrin resulted in minor to no effect on
328 BIC effector fluorescence patterns (Figure 9A-C). Two chemical inhibitors with potential CME
329 association (Table 1) show different impacts on BIC effector fluorescence patterns. Wortmannin,
330 which inhibits phosphatidylinositol 3-kinase (PI 3-kinase) and is implicated in late endosomal
331 trafficking (Robinson et al., 2008) had a major impact on BIC structure, while concanamycin A,
332 which inhibits vacuolar-type ATPase and induces vacuolar acidification (Robinson et al., 2008),
333 had little impact on BIC structure (Figure 9A-C).

334 Moreover, treatment with CME inhibitors cantharidin, chlorpromazine and triclosan, but
335 not with CIE inhibitors filipin and methyl-β-cyclodextrin, resulted in reduced appressorial
336 penetration and induced abnormal accumulation of the cytoplasmic effector Pwl2:mRFP under
337 appressorial penetration sites where it is not normally observed (Figure 9A - compare 18 hpi CIE
338 and CME inhibitors; Figure 9D,E). Wortmannin, but not concanamycin A, also impacted
339 appressorial function and resulted in abnormal Pwl2:mRFP accumulation under appressoria. These
340 results support our findings with Bas170:mRFP (Figure 1D-F) in suggesting that effector uptake
341 begins before or at the point that host penetration occurs. Indeed, chemical inhibition of
342 endocytosis in rice cells undergoing *M. oryzae* infection mimics the results obtained with VIGS,
343 further supporting a role for CME in effector uptake into rice cells.
344

345 **DISCUSSION**

346 Our results, when taken together, provide strong evidence that cytoplasmic effector translocation
347 is BIC-localized and mediated by CME. We report that diverse cytoplasmic effectors occur in
348 dynamic vesicles in tip-BICs associated with primary hyphae that first colonize host cells and then
349 in BICs that remain beside the first bulbous IH after hyphal differentiation. Tip-BICs contain many
350 small effector micro-vesicles (~87 nm) and co-expression of differentially-labeled effectors
351 Bas1:eYFP and Pwl2:mRFP showed these effectors can be sorted into different vesicles (Figure
352 2). Vesicle composition can be seen to vary as tip-BICs move to become side-BICs during hyphal
353 differentiation. Specifically, side-BICs contained fewer, larger vesicles that reach >500 nm in
354 diameter and show co-localization of Bas1:eYFP and Pwl2:mRFP. Our results confirm a previous
355 report that cytoplasmic effectors occur in ~500 nm vesicles in the outer BIC domes beside bulbous
356 IH (Mochizuki et al., 2015; Nishimura et al., 2016; Nishizawa et al., 2016). We also observed
357 effector vesicles in the host cytoplasm at short distances from maturing side-BICs (Figure 2).
358 Release of effectors from these vesicles into the host cytoplasm would require a special
359 mechanism, perhaps mediation by an effector as suggested for release of the *S. parasitica* effector
360 from endocytic vesicles into the fish cell cytoplasm (Trusch et al., 2018).

361 We report that BICs producing effector vesicles contain multiple hallmarks of active
362 clathrin-mediated endocytosis (CEM), including focal accumulation of fluorescently-labelled
363 Clathrin Light Chain-1 (CLC1), a key subunit of the clathrin coat in CME (Figure 6). Focal
364 accumulation of actin in the BICs, as detected in stable transgenic plants expressing LifeAct:eGFP

365 and by staining with rhodamine-labeled phalloidin (Figure 5), is consistent with a role in CME,
366 although it was recently reported that actin plays a different role in CME in plants than in the well-
367 studied systems in mammals and yeast (Qi et al., 2018; Johnson et al., 2020; Narasimhan et al.,
368 2020). We confirm that BICs contain abundant rice plasma membrane (Giraldo et al., 2013) using
369 transgenic plants expressing fluorescent plasma membrane fusion protein LTi6b:eGFP, and using
370 the amphiphilic stryryl dyes FM 4-64 or FM 1-43 to track membranes that are internalized by
371 endocytosis (Bolte et al., 2004). Indeed, we obtained occasional views of effector vesicles ringed
372 in LTi6b:eGFP or FM 4-64 labeled membrane (Figure 3C). Interestingly, we identified a novel
373 effector, Bas83, that labels non-effector vesicles and EIHM focused around BICs and the BIC-
374 associated cells, which could be involved in replenishing host membranes needed for extensive
375 endocytotic activity in the BIC (Figure 4; Supplemental Figure S3). In contrast, flotillin
376 (Flot1:eGFP), which is a component of lipid raft-mediated clathrin independent endocytosis, rarely
377 co-localizes with tip-BICs where active translocation is occurring (Figure 6C). Our fluorescent
378 marker co-localization experiments are all consistent with BICs as a focused area of CME.

379 For functional analyses of the role of endocytosis in effector translocation, we performed
380 transient silencing of two rice CME components, Clathrin Heavy Chain-1 (CHC-1) and Adaptor
381 Protein Complex subunit 2α (AP-2α), as well as silencing of the CIE component Flotillin-1. We
382 also used 7 pharmacological agents that are reported to inhibit or be associated with CME or CIE
383 in plants. Both strategies have potential problems. Rice plants that received the CHC-1 and APC-
384 2 silencing vectors were significantly reduced in rice blast symptom, compared to the empty vector
385 control and to Flot1-silenced lines (Figure 7; Supplemental Figure S5). However, this could be
386 due, at least in part to inevitable health costs to the plant through silencing component genes for
387 essential cellular processes. Unhealthy rice plants are generally less susceptible to blast disease
388 (Kato, 1974). Additionally, care must be taken in the interpretation of results in pharmacological
389 studies based on new evidence that endocytosis inhibitors characterized in mammalian systems
390 may not have the same targets in plants (Dejonghe et al., 2016), and pharmacological agents also
391 have off-target effects (Hicks and Raikhel, 2010; Dejonghe and Russinova, 2017). However, both
392 studies complement each other in that transient silencing of the two CME components and
393 treatment with 4 different pharmacological agents associated with CME gave the same swollen
394 BIC phenotype, in which labeled fluorescent effectors accumulate in abnormally-sized BICs
395 lacking the discreet effector vesicles seen in control infection sites (Figures 7-9). In contrast,

396 transient silencing of the CIE component Flotilin-1 and treatment with pharmacological inhibitors
397 associated with CIE show little or no impact on BIC vesicular structure and pathogenicity (Figure
398 8 and 9). All results from our VIGS and chemical inhibitor experiments are consistent with our
399 fluorescence localization experiments. Taken together, our results therefore provide evidence that
400 BICs include a focused region of plant clathrin-mediated endocytosis for internalizing cytoplasmic
401 effectors inside living plant cells (Figure 10).

402 We report two new lines of evidence that effectors are being secreted and translocated into
403 the host cytoplasm from appressoria even before obvious growth of primary hyphae inside host
404 cells. First, we identified an effector, Bas170, that naturally accumulates in host nuclei before
405 visible growth of primary hyphae, and it also localizes to vesicles underneath appressoria at this
406 early time point. Second, effector Pwl2:mRFP, which is not normally observed before the tip-BIC
407 stage, accumulates under appressoria that failed to penetrate after both VIGS silencing and
408 chemical inhibition of rice CME. These new findings are consistent with reports that rice cells
409 recognize and respond to *M. oryzae* before and independently of appressorial penetration (Xu et
410 al., 1998). It has been predicted that *M. oryzae* appressorial pores, a transient cell wall-less region
411 of the appressorium adjacent to the plant cuticle, might be involved in molecular communication
412 between pathogen and host before penetration (Howard and Valent, 1996). Previously, the only
413 *M. oryzae* effector that was a candidate for secretion through the appressorial pore was a presumed
414 secondary metabolite that is produced by the *AVR* gene *ACE1* encoding a hybrid polyketide
415 synthase (PKS) and nonribosomal peptide synthetase (NRPS) that is specifically expressed in the
416 cytoplasm of appressoria before and during penetration (Fudal et al., 2007; Collemare et al., 2008).
417 Therefore, our new effector localization results suggest similar exquisite staging of effector
418 expression as reported for the crucifer pathogen *Colletotrichum higginsianum*, which secretes
419 ChEC effectors under the appressorial pores and at subsequent stages during the invasion of
420 *Arabidopsis thaliana* cells (Kleemann et al., 2012). Specifically, this fungus focally secreted
421 effectors Chec6 and Chec36 from the appressorium pore, suggesting these effectors may be
422 translocated before fungal penetration (Kleemann et al., 2012). Our results with Bas170 together
423 with ChECs and Ace1 protein localization patterns indicate that many effectors might be focally
424 secreted through appressorial pores (Fudal et al., 2007; Kleemann et al., 2012), highlighting a
425 potential role for fungal appressoria in effector delivery.

426 The effector vesicle dynamics that we report support the idea that front-loaded effector
427 translocation occurs during the early stages of host cell invasion. Specifically, tip-BIC vesicles are
428 small (~87 nm), abundant and selective in terms of sorting different cytoplasmic effectors,
429 Bas1:eYFP and Pwl2:mRFP, into different vesicles. In contrast, side-BICs contain fewer, larger,
430 less-selective vesicles that contain both Bas1:eYFP and Pwl2:mRFP. Effector vesicles observed
431 in the cytoplasm were almost uniformly found at the side-BIC stage, perhaps indicating a slow-
432 down of the mechanism for effector release from the vesicles as BICs mature. The mechanism for
433 forming vesicles may result in larger vesicles, or vesicles may fuse before releasing effectors to
434 the cytoplasm in the later BIC stages. Slowdown of the translocation system would appear
435 consistent with previous reports of loss of activity in BICs as host cells fill with IH (Khang et al.,
436 2010; Jones et al., 2021). Front-loading effector translocation from BICs would make sense
437 because cell-to-cell movement of blast cytoplasmic effectors through plasmodesmata must occur
438 in the early stages of host cell invasion while the EIHM enclosing the IH remains intact and
439 plasmodesmata in the invaded cell remain open (Sakulkoo et al., 2018; Jones et al., 2021). Active
440 BICs are surrounded by host cytoplasm with dynamic connections to the cell periphery (Khang et
441 al., 2010; Supplemental Movie S2), where cytoplasmic streaming would rapidly disperse effectors
442 to pit fields containing plasmodesmata. In contrast, nonBIC-associated IH cells invaginate the host
443 vacuole and grow in close proximity to the host vacuolar membrane with little surrounding
444 cytoplasm (Mochizuki et al., 2015; Jones et al., 2021). Specifically, the host vacuole remains
445 intact, but shrinks as IH grow. Both the EIHM and vacuolar membrane become disrupted,
446 indicating death of the invaded cell, around the time IH move into neighboring cells to repeat their
447 BIC-mediated invasion strategy (Mochizuki et al., 2015; Jones et al., 2021).
448 There is evidence supporting occurrence of clathrin-mediated endocytosis at the EHM in
449 one additional pathosystem. That is, transmission electron micrographs of the interfacial matrix
450 between the intracellular hyphae [called monokaryotic (M)-haustoria] of the monokaryotic rust
451 fungus *Uromyces vignae* and its host cowpea (*Vigna unguiculata*) shows clathrin-coated pits
452 (diameter ca. 50-70nm) on the EHM at M-haustoria hyphal tips that contained dense cytoplasm
453 and were presumably growing (Stark-Urnau and Mendgen, 1995). The coated vesicles were
454 labeled by an antibody recognizing the heavy chain subunit of clathrin. Long tubules extending
455 into the host cytoplasm, as well as coated vesicles in the surrounding host cytoplasm, were also
456 labeled with the antibody, indicating that endocytosis occurs at the EHM (Stark-Urnau and

457 Mendgen, 1995; O'Connell and Panstruga, 2006). It was suggested that these endocytic vesicles
458 might be involved in effector uptake into host cells in addition to membrane recycling from host
459 exocytosis. Unfortunately, lack of transformation capability and identification of effectors makes
460 it difficult to follow up on these intriguing results with *U. vignae*. Additional TEM studies support
461 our results that transient silencing of lipid raft-mediated endocytosis component Flotilin1, as well
462 as filipin treatment, had little effect on BIC structure and effector vesicle formation. Freeze-
463 fracture transmission electron microscopy (TEM) following filipin treatment revealed an absence
464 of granular filipin-sterol complexes on the EHM of two rust fungi, *Puccinia coronata* and
465 *Uromyces appendiculatus* (Harder and Mendgen, 1982), suggesting that the extrahaustorial
466 membrane contains less sterol than normal plasma membranes, and indicating that the EHM
467 appears depleted in sterol-rich lipid rafts.

468 Differences in infection strategies among various filamentous biotrophic or hemibiotrophic
469 pathogens would be consistent with use of different strategies for effector translocation in different
470 pathosystems. A recent report indicates that a complex of seven proteins from the smut pathogen
471 *U. maydis* is critical for infection and implicated in translocation of cytoplasmic effectors into
472 maize cells (Ludwig et al., 2021). This basidiomycete fungus colonizes host tissue as intracellular
473 hyphae that pass through and between host cells without obviously specialized interfacial zones,
474 and fluorescent fusion proteins of cytoplasmic effectors have not been visualized in the host cell
475 cytoplasm in this pathosystem (Lo Presti et al., 2017). *U. maydis* produces galls on maize seedlings
476 and grows systemically as the plant grows to finally invade ovaries, which swell into dramatic
477 sporulating galls. In contrast, *M. oryzae* densely colonizes a localized tissue area that will become
478 a visible eyespot lesion that releases spores to reinitiate the infection cycle within 7 days. Different
479 pathogenic lifestyles could present different demands for cytoplasmic effector translocation.

480 Taken together, our data strongly suggest that clathrin-mediated endocytosis occurring in
481 BICs is a key mechanism for internalization of *M. oryzae* effectors inside living rice cells,
482 beginning even before appressorium penetration on the host surface. Given this current
483 understanding, important unknowns for future study include the molecular mechanisms of how the
484 endocytic machinery is recruited to BICs and how it interacts with effector cargos (Qi et al., 2018),
485 including how different effectors are sorted out into different vesicles as shown in Figure 2. It is
486 important to understand vesicle dynamics through time and why effector vesicles become larger
487 and less selective as BICs mature. It is important to understand if, and if so, how, Bas83 contributes

488 to membrane recruitment to BICs and the EIHM surrounding BIC-associated cells. It is unknown
489 how the effector vesicles are disrupted, releasing effectors into the rice cytoplasm and how various
490 effectors are then targeted to their destinations in host cells including, in some cases, movement
491 through plasmodesmata into neighboring host cells. It is also important to understand the role for
492 appressoria in effector secretion before penetration, and how these early effectors, such as the host
493 nuclear localized effector Bas170, function to promote infection. Finally, it is critical to translate
494 molecular mechanisms of blast biotrophic invasion into strategies for controlling devastating
495 diseases on rice, wheat and other food crops worldwide.
496

497 **METHODS**

498 **Live-cell imaging of *M. oryzae* effectors *in planta***

499 Fungal strains were stored in dried filter papers at -20˚C, and cultured on rice polish agar plates at
500 25˚C under continuous light for 2 weeks (Valent and Chumley, 1991). Rice sheath inoculations
501 were performed as described (Kankanala et al., 2007) with the following modification. We used
502 sheath pieces that were thickly trimmed (~7 rice cell layers thick) compared to thinner trimmed
503 sheaths (~3 cell layers thick) in previous publications. Brightfield images were less detailed, but
504 the endocytic machinery appeared more active, providing enhanced microscopic resolution of
505 fluorescent marker dynamics. Susceptible rice variety YT-16 was used unless mentioned
506 otherwise. Briefly, 7-cm-long sheath pieces from 3-week-old plants were placed in a sealable
507 Pyrex glass moist chamber. Leaf sheath sections were placed on inverted 8-well PCR tube strips
508 to avoid contact with wet paper and to hold epidermal cells directly above the mid-vein
509 horizontally flat for uniform inoculum distribution in the trimmed sheath pieces. A spore
510 suspension (10^4 spores/ml in sterile 0.25% gelatin, Cat. #G-6650, Sigma-Aldrich) was prepared
511 from 10-day old cultures and was injected into one end of the sheath using a 100-ml pipette. Each
512 segment was trimmed at 18–30 h.p.i., treated with specific dyes or inhibitors, or imaged
513 immediately by laser confocal microscopy. Confocal imaging was performed with a Zeiss
514 LSM780 confocal microscope system using two water immersion objectives, C-Apochromat
515 40x/1.2 WCorr. and C-Apochromat 63x/1.2WCorr. Excitation/emission wavelengths were 488
516 nm/505–550 nm for eGFP and FM1-43, and 543 nm/560–615 nm for mRFP, mCherry, Phalloidin
517 and FM4-64. Images were acquired and processed using Zeiss ZEN 2010 software. Images of
518 effector vesicles in Figure 3C were obtained using a Leica SP8 confocal microscope system with

519 a water immersion objective HC PL APO 63x/1.20 WCorr. Excitation/emission wavelengths were
520 488 nm/505–550 nm for eGFP and 543 nm/560–615 nm for mRFP.

521 **Fungal strains, DNA manipulation, and fungal transformation**

522 *Magnaporthe oryzae* wild type strain Guy11, a field isolate from rice in French Guiana, was
523 obtained from J.L. Notteghem (Centre de Cooperation Internationale en Recherche Agronomique
524 pour le Developpment). *M. oryzae* transformants are described in Supplemental Table S1 online.
525 Effector:mRFP and Effector:eGFP expression plasmids were constructed by PCR amplifying
526 different effector gene regions and fusing them to the N-terminus of mRFP and eGFP, respectively.
527 Details of construction of each plasmid are described in Supplemental Table S2, and primers are
528 listed in Supplemental Table S3. For all fusion constructs, transcriptional and translational fusions
529 were verified by DNA sequencing. See Supplemental Table S2 online for plasmids used, and
530 Supplemental Table S3 for PCR primers used. Plasmids were transformed into laboratory strain
531 Guy11 (Leung et al., 1988) using *Agrobacterium tumefaciens*–mediated transformation (Khang et
532 al., 2006). In several cases, two fluorescently labelled effectors were introduced by co-
533 transformation with separate plasmids (Sweigard et al., 1995). Because positive transformants
534 showed similar fluorescence patterns with varying intensities, those with strongest fluorescence
535 were studied (see Supplemental Table S1 online). For each construct cloned in *M. oryzae*, at least
536 two independent transformants showing identical phenotypes to the wild type were selected and
537 assayed together.

538 **Strategies for targeted deletion of Bas83 gene**

539 *Split-marker recombination method for Bas83 gene knockout via protoplast transformation*:
540 Targeted gene replacement mutation of the *M. oryzae Bas83* gene was attempted using the split
541 marker strategy as modified by Kershaw and Talbot (2009). Gene replacement was performed by
542 replacing the 606-bp *Bas83* locus with a hygromycin resistance selectable marker, encoding a 1.4-
543 kb hygromycin phosphotransferase (*HPH*) resistance cassette (Carroll et al., 1994). The two
544 overlapping segments of the *HPH* templates were PCR amplified using primers M13F with HY
545 and M13R with YG (Catlett et al., 2003) (see Supplemental Table S3 online) as described
546 previously (Kershaw and Talbot, 2009). One-kb DNA fragments upstream and downstream of the
547 *Bas83* open reading frame were generated using the primers Bas83LF-F and Bas83LFHY-R and
548 Bas83RFYG-F and Bas83RF-R amplified from genomic DNA of the Guy11 strain. A second-

549 round PCR reaction was performed to fuse the overlapping split hph marker templates with the
550 left and right flanking regions of the Bas83 locus. Wild-type *M. oryzae* strain Guy11 was then
551 transformed with the deletion cassettes (2 µg of each flank). Putative transformants were selected
552 in the presence of hygromycin B (200 µg/ml) and analyzed by PCR using the primers
553 Bas83:BASKOtest-F and Bas83:BASKOtest-R (Supplemental Table S3; Supplemental Figure
554 S4). This assay was repeated three times. Gene sequences on either side of *Bas83* were retrieved
555 from the NCBI database (https://www.ncbi.nlm.nih.gov/).

556 *Attempted Bas83 deletion via Agrobacterium-mediated transformation*: For gene
557 replacement transformation, cassettes were constructed by amplifying ~1.0 kb of 5′- and 3′-
558 flanking regions for each predicted coding sequence. The *HPH* gene (Carroll et al., 1994) was
559 cloned between the two flanking regions using a fusion PCR strategy. The three pieces together
560 were cloned first into the pJET1.6 vector (Invitrogen) for sequence analysis and later into binary
561 vector pGKO2 (Addgene: Plasmid #63617; Khang et al., 2005) using a restriction ligation strategy.
562 *M. oryzae* KU70 and KU80 spores were transformed using *A. tumefaciens* (Khang et al., 2005)
563 strains AGL1 and EHA105 (Hellens et al., 2000). After two rounds of selection in TB3 media
564 containing 200 µg/mL of hygromycin, 400 independent fungal transformants were analyzed for
565 gene replacement events by PCR amplification using the primers Bas83:BASKOtest-F and
566 Bas83:BASKOtest-R (Supplemental Figure S4). This assay was repeated three times.

567 **Staining with FM 4-64, FM 1-43, and Rhodamine Phalloidin, and treatment with**
568 **pharmacological inhibitors**

569 To examine membrane dynamics at the BIC, rice sheaths (cv. YT16) were inoculated with *M.*
570 *oryzae* transformants expressing fluorescently-labeled effectors ($2x10^4$ spores/ml in 0.25% gelatin
571 solution) and incubated for 20-26 hours at 25˚C for subsequent FM-dye treatment. Infected rice
572 sheaths were treated with FM 4-64 or FM 1-43 (4 mg/ml in water). An aqueous 17mM stock
573 solution of FM 4-64 (Cat #13320, Invitrogen, Carlsbad, CA) and FM 1-43 (Cat # T3163,
574 Invitrogen, Carlsbad, CA) were prepared and stored at -20˚C as described (45). *In planta*,
575 inoculated leaf sheaths, 24 h.p.i., were trimmed into ultrathin sections (2-3 layers of cells; 10 x 10
576 mm) and incubated in a 10-mM aqueous working solution for 3–5 hours. Leaf sheaf sections were
577 subsequently transferred to ultrapure water and incubated for 20 min (25 ˚C) to remove excess
578 dyes for uniform membrane staining. For *in planta* experiments with Rhodamine Phalloidin (Cat#
579 R415, ThermoFisher Scientific), we prepared working solutions of 66 µM in 0.1% DMSO and

580 treated the inoculated tissue as described for FM dyes.

581 To examine the effects of endocytosis inhibitors on *in planta* effector uptake, inoculated
582 trimmed rice sheaths were incubated at 25˚C with Methyl-β-cyclodextrin (20 mM), or
583 Chlorpromazine (10 µg/mL), or Cantharidin (25 mM), or Fluazinam (20 mM), or Triclosan
584 (20mM), or Wortmannin (20 nM), or Concanamycin A (50 mM) (all from Sigma) solution for 1-
585 5 hours. Negative controls were performed with ultrapure water (Methyl-β-cyclodextrin,
586 Chlorpromazine, and Fluazinam) or 0.1% DMSO (Cantharidin, Filipin and Wortamanin) (see
587 Table 1).

588 **Generation of transgenic rice plants**

589 Production of transgenic plants expressing the plant plasma membrane marker low-temperature
590 inducible protein 6B, LTi6B:GFP was previously described (Mentlak et al., 2012; Giraldo et al.,
591 2013). Transformants of rice cultivar Sasanishiki expressing LifeAct:eGFP were generated in the
592 laboratory of NJT. Expression plasmids for CME and CIE marker genes were constructed by PCR
593 amplifying the marker gene regions and fusing them to the N-terminus of eGFP. The *CLC1* gene
594 was amplified from genomic DNA of YT16 rice using the primers KpnI_OsCLC1Prom1-F1 and
595 XhoI_OsCLC1-R1. The PCR product was digested with *Kpn*I and *Xho*I and integrated into
596 pSH1.6EGFP (Plasmid #42323, Addgene). The *Flot1* gene was amplified from genomic DNA
597 from YT16 rice using the primers HindIII_OsFlot1Prom1-F1 and Eco47III_OsFlot-R1. The PCR
598 product was digested with *Hind*III and *Eco*47III and integrated into pSH1.6EGFP. CLC1:eGFP
599 was amplified from pSH1.6_CLC1:eGFP using the primers CACC_OsCLC1-F1 and eGFPT2-R2,
600 and cloned into pENTR (pENTR™/D-TOPO™ Cloning Kit, ThermoFisher Scientific) following
601 the manufacturer's protocol. Flot1:eGFP was amplified form pSH1.6_Flot1:eGFP using the
602 primers CACC_OsFlot1-F1 and eGFPT2-R2, and cloned into pENTR following manufacturer's
603 protocols. Endocytosis marker:eGFP construct were cloned into the *Agrobacterium* vector
604 pIPKb001 (Himmelbach et al., 2007) using the Gateway LR Clonase II kit (Invitrogen) following
605 the manufacturer's protocol. All the fusion constructs had transcriptional and translational fusions
606 verified by DNA sequencing. Gene fusions for expressing the rice endocytosis markers
607 CLC1:eGFP (CME) and Flot1:eGFP (CIE) under their native promoters were introduced into
608 *Agrobacterium tumefaciens* EHA105 using the freeze-thaw method (Holsters et al., 1978). Mature
609 seed-derived callus from rice (*Oryza sativa L. Japonica*) cv. YT16 was used for *Agrobacterium*-
610 mediated transformation (Park et al., 2001). After inoculating with *A. tumefaciens*, callus was

611 transferred to regeneration medium for 4-10 weeks at 25˚C under a 16-h photoperiod. The
612 regenerated shoots were transferred to rooting medium for four more weeks, then established in
613 soil. Putative transformants of rice were selected on 100 µg/ml hygromycin, and expression
614 checked by qRT–PCR and epifluorescence microscopy.

615 **Silencing of rice genes**

616 In order to evaluate the role of plant endocytosis on disease development and effector uptake, we
617 performed VIGS using the Brome mosaic virus system developed by R.S. Nelson (Noble
618 Foundation, Ardmore, OK). We targeted *AP-2α*, *CHC1* (CME) and *Flot1* (CIE) mRNA in rice
619 plants (cultivar IR64) undergoing infection. The target rice sequences were cloned in the pC13/F3-
620 13m VIGS vector as described (Ding et al., 2006; Ding et al., 2007) and subsequently sequenced
621 to verify sequence accuracy. RNA transcripts were synthesized from the final VIGS vector. An
622 empty vector pC13/F3-13m was used as negative control. The final infectious transcripts of
623 pC13/F3-13m / AP-2α, pC13/F3-13m / CHC1, pC13/F3-13m /Flot1 and pC13/F3-13m (a control
624 virus without an insert) were inoculated with pC13/F1+2 in 7 to 10 day old IR64 rice plants
625 according protocols described by Ding et al (2006). Knockdown of the target genes was confirmed
626 by qRT-PCR at 15 days post inoculation. At this point, rice plants showing satisfactory reduction
627 of the transcription levels were used in our standard conidial spray inoculation and leaf sheath
628 assays with fungal strains expressing fluorescently-labeled effectors.

629 **Statistics**

630 All experiments were performed in triplicate and repeated three times. The sample sizes, number
631 of biological and technical replicates, and the statistical tests used in each experiment are specified
632 in the figure legends. Data were analyzed using an unpaired two-tailed Student's t-test. P=0.05
633 was considered non-significant and exact values are shown where appropriate. All statistical
634 analysis was performed using R Statistical Software (version 4.1.2) and Prism9 (GraphPad). The
635 linescans in Figure 8 were used to illustrate cytoplasmic effector accumulation due to CME
636 inhibition and compared to the apoplastic effector Bas4 (control). Dot plots were routinely used to
637 show individual data points and generated using Prism9 (GraphPad). Bar graphs show the
638 mean±s.e.m. (unless stated otherwise) and were generated using Prism9 (GraphPad). Analysis of
639 non-normal datasets are represented by box-and-whisker plots that show the 25th and 75th

640 percentiles, the median indicated by a horizontal line, and the minimum and maximum values
641 indicated by the ends of the whiskers.
642
643 **Accession Numbers**
644 Sequence data for genes of *M. oryzae* used in this article can be found in the GenBank/EMBL
645 database under the following accession numbers: BAS1, NC_017844; PWL1, U36923.1; PWL2,
646 NC_017853; Bas4, NC_017852.1; BAS83, NC_017851.1; BAS170, NC_017850.1. Rice genes
647 used are: Clathrin Light Chain-1 (CLC1), LOC4337419; Flotilin 1 (Flot1), LOC4348926; Adaptor
648 protein complex-2α (AP-2α), LOC4331370; and Clathrin Heavy Chain-1 (CHC1 gene;
649 LOC4349546.
650
651 **ACKNOWLEDGEMENTS**
652 We acknowledge and thank Rick Nelson (Noble Foundation, Ardmore, OK) for providing the
653 VIGS vectors and hosting E.O.-G. in his laboratory to learn the VIGS assay. We thank the Talbot
654 laboratory for assistance and hospitality during a working visit for E.O.-G at the University of
655 Exeter. We thank Hiromasa Saitoh (Iwate Biotechnology Research Center, Kitakami, Iwate,
656 Japan) and Ryohei Terauchi (Iwate Biotechnology Research Center, Kitakami, Iwate, and Kyoto
657 University, Japan) for sharing transgenic rice expressing plant plasma membrane marker
658 LTi6B:GFP. This project was supported by Agriculture and Food Research Initiative Competitive
659 Grant no. #2017-67013-26525 from the USDA National Institute of Food and Agriculture Plant
660 Biotic Interactions program. This is Contribution no. 22-053-J from the Kansas Agricultural
661 Experiment Station.
662
663 **AUTHOR CONTRIBUTIONS**
664 E.O.-G. and B.V. designed experiments and analyzed data: E.O.-G. performed most of the
665 research. T.M.T., J.P. and S.P. produced and analyzed transgenic rice lines expressing the rice
666 CLC1:eGFP and Flot1:eGFP fluorescent fusion protein genes. M.D., M.M.-U., C.R.H. and A.H.V.
667 assisted with microscopy and Bas83 Knockout experiments and general laboratory experiments;
668 N.J.T. provided transgenic rice lines expressing LTi6B:GFP and LifeACT:GFP; E.O.-G., B.V. and
669 N.J.T wrote and edited the article.
670

671 **REFERENCES**

672 Atkinson, H.A., Daniels, A., and Read, N.D. 2002. Live-cell imaging of endocytosis during
673 conidial germination in the rice blast fungus, *Magnaporthe grisea*. Fungal Gen. Biol. 37:233-
674 244.

675 Beck, M., Heard, W., Mbengue, M., and Robatzek, S. 2012. The INs and OUTs of pattern
676 recognition receptors at the cell surface. Curr. Opin. Plant Biol. 15:367-374.

677 Bolte, S., Talbot, C., Boutte, Y., Catrice, O., Read, N.D., and Satiat-Jeunemaitre, B. 2004. FM-
678 dyes as experimental probes for dissecting vesicle trafficking in living plant cells. Journal of
679 Microscopy 214:159-173.

680 Bozkurt, T.O., Belhaj, K., Dagdas, Y.F., Chaparro-Garcia, A., Wu, C.-H., Cano, L.M., and
681 Kamoun, S. 2015. Rerouting of plant late endocytic trafficking toward a pathogen interface.
682 Traffic 16:204-226.

683 Bright, N.A., Lindsay, M.R., Stewart, A., and Luzio, J.P. 2001. The relationship between lumenal
684 and limiting membranes in swollen late endocytic compartments formed after wortmannin
685 treatment or sucrose accumulation. Traffic 2:631-642.

686 Carroll, A., Sweigard, J. A., and Valent, B. 1994. Improved vectors for selecting resistance to
687 hygromycin. 41:Article 5. https://newprairiepress.org/fgr/vol41/iss41/45/.

688 Catlett, N. L., Lee, B.-N., Yoder, O. C., and Turgeon, B. G. 2003. Split-marker recombination for
689 efficient targeted deletion of fungal genes. Fungal Genetics Newsletter 50:Article 4.
690 https://doi.org/10.4148/1941-4765.1150.

691 Chaparro-Garcia, A., Schwizer, S., Sklenar, J., Yoshida, K., Petre, B., Bos, J.I.B., Schornack, S.,
692 Jones, A.M.E., Bozkurt, T.O., and Kamoun, S. 2015. *Phytophthora infestans* RXLR-WY
693 effector AVR3a associates with dynamin-related protein 2 required for endocytosis of the
694 plant pattern recognition receptor FLS2. PLoS ONE 10:e0137071.

695 Chen, X., Irani, N.G., and Friml, J. 2011. Clathrin-mediated endocytosis: the gateway into plant
696 cells. Curr. Opin. Plant Biol. 14:674-682.

697 Collemare, J., Pianfetti, M., Houlle, A.E., Morin, D., Camborde, L., Gagey, M.J., Barbisan, C.,
698 Fudal, I., Lebrun, M.H., and Böhnert, H.U. 2008. *Magnaporthe grisea* avirulence gene *ACE1*
699 belongs to an infection-specific gene cluster involved in secondary metabolism. New Phytol.
700 179:196-208.

701 Dagdas, Y.F., Pandey, P., Tumtas, Y., Sanguankiattichai, N., Belhaj, K., Duggan, C., Leary, A.Y.,
702 Segretin, M.E., Contreras, M.P., Savage, Z., Khandare, V.S., Kamoun, S., and Bozkurt, T.O.
703 2018. Host autophagy machinery is diverted to the pathogen interface to mediate focal
704 defense responses against the Irish potato famine pathogen. eLife 7:e37476.
705 Dejonghe, W., and Russinova, E. 2017. Plant chemical genetics: From phenotype-based screens
706 to synthetic biology. Plant Physiology 174:5-20.
707 Dejonghe, W., Kuenen, S., Mylle, E., Vasileva, M., Keech, O., Viotti, C., Swerts, J., Fendrych,
708 M., Ortiz-Morea, F.A., Mishev, K., Delang, S., Scholl, S., Zarza, X., Heilmann, M., Kourelis,
709 J., Kasprowicz, J., Nguyen, L.S.L., Drozdzecki, A., Van Houtte, I., Szatmári, A.-M., Majda,
710 M., Baisa, G., Bednarek, S.Y., Robert, S., Audenaert, D., Testerink, C., Munnik, T., Van
711 Damme, D., Heilmann, I., Schumacher, K., Winne, J., Friml, J., Verstreken, P., and
712 Russinova, E. 2016. Mitochondrial uncouplers inhibit clathrin-mediated endocytosis largely
713 through cytoplasmic acidification. Nat. Comm. 7:11710.
714 Di Rubbo, S., Irani, N. G., Kim, S. Y., Xu, Z.-Y., Gadeyne, A., Dejonghe, W., Vanhoutte, I.,
715 Persiau, G., Eeckhout, D., Simon, S., Song, K., Kleine-Vehn, J., Friml, J., De Jaeger, G., Van
716 Damme, D., Hwang, I., and Russinova, E. 2013. The Clathrin Adaptor Complex AP-2
717 mediates endocytosis of BRASSINOSTEROID INSENSITIVE1 in *Arabidopsis*. Plant Cell
718 25:2986-2997.
719 Ding, X.S., Rao, C.S., and Nelson, R.S. 2007. Analysis of gene function in rice through virus-
720 induced gene silencing. Methods in molecular biology (Clifton, N.J.) 354:145-160.
721 Ding, X.S., Schneider, W.L., Chaluvadi, S.R., Mian, M.A.R., and Nelson, R.S. 2006.
722 Characterization of a Brome mosaic virus strain and its use as a vector for gene silencing in
723 monocotyledonous hosts. Mol. Plant-Microbe Interact. 19:1229-1239.
724 Dodds, P.N., and Rathjen, J.P. 2010. Plant immunity: towards an integrated view of plant-pathogen
725 interactions. Nat. Rev. Genet. 11:539-548.
726 Elsworth, B., Matthews, K., Nie, C.Q., Kalanon, M., Charnaud, S.C., Sanders, P.R., Chisholm,
727 S.A., Counihan, N.A., Shaw, P.J., Pino, P., Chan, J.A., Azevedo, M.F., Rogerson, S.J.,
728 Beeson, J.G., Crabb, B.S., Gilson, P.R., and de Koning-Ward, T.F. 2014. PTEX is an
729 essential nexus for protein export in malaria parasites. Nature 511:587-+.
730 Ewers, H., and Helenius, A. 2011. Lipid-mediated endocytosis. Cold Spring Harbor Perspectives
731 in Biology 3:10.1101/cshperspect.a004721.

732 Fan, L., Li, R., Pan, J., Ding, Z., and Lin, J. 2015. Endocytosis and its regulation in plants. Trends
733 in Plant Science 20:388-397.
734 Fawke, S., Doumane, M., and Schornack, S. 2015. Oomycete interactions with plants: infection
735 strategies and resistance principles. Microbiology and Molecular Biology Reviews 79:263-
736 280.
737 Fudal, I., Collemare, J., Böhnert, H.U., Melayah, D., and Lebrun, M.-H. 2007. Expression of
738 *Magnaporthe grisea* avirulence gene *ACE1* is connected to the initiation of appressorium-
739 mediated penetration. Eukaryotic Cell 6:546-554.
740 Giraldo, M.C., and Valent, B. 2013. Filamentous plant pathogen effectors in action. Nat. Rev.
741 Microbiol. 11:800-814.
742 Giraldo, M.C., Dagdas, Y.F., Gupta, Y.K., Mentlak, T.A., Yi, M., Martinez-Rocha, A.L., Saitoh,
743 H., Terauchi, R., Talbot, N.J., and Valent, B. 2013. Two distinct secretion systems facilitate
744 tissue invasion by the rice blast fungus *Magnaporthe oryzae*. Nat. Comm. 4:1996.
745 Gladieux, P., Condon, B., Ravel, S., Soanes, D., Maciel, J.L.N., Nhani, A., Chen, L., Terauchi, R.,
746 Lebrun, M.-H., Tharreau, D., Mitchell, T., Pedley, K.F., Valent, B., Talbot, N.J., Farman,
747 M., and Fournier, E. 2018. Gene flow between divergent cereal- and grass-specific lineages
748 of the rice blast fungus *Magnaporthe oryzae*. mBio 9:e01219-01217.
749 Grassart, A., Cheng, A.T., Hong, S.H., Zhang, F., Zenzer, N., Feng, Y., Briner, D.M., Davis, G.D.,
750 Malkov, D., and Drubin, D.G. 2014. Actin and dynamin2 dynamics and interplay during
751 clathrin-mediated endocytosis. Journal of Cell Biology 205:721-735.
752 Harder, D.E., and Mendgen, K. 1982. Filipin-sterol complexes in bean rust- and oat crown rust-
753 fungal/plant interactions: Freeze-etch electron microscopy. Protoplasma 112:46-54.
754 Hellens, R., Mullineaux, P., and Klee, H. 2000. Technical Focus: a guide to *Agrobacterium* binary
755 Ti vectors. Trends Plant Sci. 5:446-451.
756 Hicks, G.R., and Raikhel, N.V. 2010. Advances in dissecting endomembrane trafficking with
757 small molecules. Curr. Opin. Plant Biol. 13:706-713.
758 Himmelbach, A., Zierold, U., Hensel, G., Riechen, J., Douchkov, D., Schweizer, P., and Kumlehn,
759 J. 2007. A set of modular binary vectors for transformation of cereals. Plant Physiology
760 145:1192-1200.

761 Holsters, M., de Waele, D., Depicker, A., Messens, E., van Montagu, M., and Schell, J. 1978.
762 Transfection and transformation of *Agrobacterium tumefaciens*. Molecular and General
763 Genetics 163:181-187.
764 Howard, R.J., and Valent, B. 1996. Breaking and Entering: Host penetration by the fungal rice
765 blast pathogen *Magnaporthe grisea*. Annu. Rev. Microbiol. 50:491-512.
766 Johnson, A., Gnyliukh, N., Kaufmann, W.A., Narasimhan, M., Vert, G., Bednarek, S.Y., and
767 Friml, J. 2020. Experimental toolbox for quantitative evaluation of clathrin-mediated
768 endocytosis in the plant model *Arabidopsis*. Journal of Cell Science 133:jcs248062.
769 Jones, K., Zhu, J., Jenkinson, C.B., Kim, D.W., Pfeifer, M.A., and Khang, C.H. 2021. Disruption
770 of the interfacial membrane leads to *Magnaporthe oryzae* effector re-location and lifestyle
771 switch during rice blast disease. Frontiers in Cell and Developmental Biology
772 9:10.3389/fcell.2021.681734.
773 Kaksonen, M., and Roux, A. 2018. Mechanisms of clathrin-mediated endocytosis. Nat. Rev. Mol.
774 Cell Biol. 19:313-326.
775 Kale, S.D., Gu, B., Capelluto, D.G.S., Dou, D., Feldman, E., Rumore, A., Arredondo, F.D.,
776 Hanlon, R., Fudal, I., Rouxel, T., Lawrence, C.B., Shan, W., and Tyler, B.M. 2010. External
777 lipid PI3P mediates entry of eukaryotic pathogen effectors into plant and animal host cells.
778 Cell 142:284-295.
779 Kankanala, P., Czymmek, K., and Valent, B. 2007. Roles for rice membrane dynamics and
780 plasmodesmata during biotrophic invasion by the blast fungus. Plant Cell 19:706-724.
781 Kato, H. 1974. Epidemiology of rice blast disease. Review of Plant Protection Research 7:1-20.
782 Kershaw, M. J., and Talbot, N. J. 2009. Genome-wide functional analysis reveals that infection-
783 associated fungal autophagy is necessary for rice blast disease. Proceedings of the National
784 Academy of Sciences U.S.A. 106:15967-15972.
785 Khang, C.H., Park, S., Rho, H., Lee, Y., and Kang, S. 2006. *Agrobacterium tumefaciens*-mediated
786 transformation and mutagenesis of filamentous fungi *Magnaporthe grisea* and *Fusarium*
787 *oxysporum*. in: Agrobacterium Protocols, K. Wang, ed. Humana Press, Totowa.
788 Khang, C.H., Berruyer, R., Giraldo, M.C., Kankanala, P., Park, S.-Y., Czymmek, K., Kang, S.,
789 and Valent, B. 2010. Translocation of *Magnaporthe oryzae* effectors into rice cells and their
790 subsequent cell-to-cell movement. Plant Cell 22:1388-1403.

791 Kleemann, J., Rincon-Rivera, L.J., Takahara, H., Neumann, U., Ver Loren van Themaat, E., van
792 der Does, H.C., Hacquard, S., Stüber, K., Will, I., Schmalenbach, W., Schmelzer, E., and
793 O'Connell, R.J. 2012. Sequential delivery of host-induced virulence effectors by appressoria
794 and intracellular hyphae of the phytopathogen *Colletotrichum higginsianum*. PLoS Path.
795 8:e1002643.
796 Konopka, C.A., Backues, S.K., and Bednarek, S.Y. 2008. Dynamics of Arabidopsis Dynamin-
797 Related Protein 1C and a Clathrin Light Chain at the plasma membrane. Plant Cell 20:1363-
798 1380.
799 Larson, E. R., Van Zelm, E., Roux, C., Marion-Poll, A., and Blatt, M. R. 2017. Clathrin heavy
800 chain subunits coordinate endo- and exocytic traffic and affect stomatal movement. Plant
801 Physiol. 175:708-720.
802 Leung, H., Borromeo, E.S., Bernardo, M.A., and Notteghem, J.L. 1988. Genetic analysis of
803 virulence in the rice blast fungus *Magnaporthe grisea*. Phytopathology 78:1227-1233.
804 Li, R., Liu, P., Wan, Y., Chen, T., Wang, Q., Mettbach, U., Baluška, F., Samaj, J., Fang, X., Lucas,
805 W.J., and Lin, J. 2012. A membrane microdomain-associated protein, *Arabidopsis* Flot1, is
806 involved in a clathrin-independent endocytic pathway and is required for seedling
807 development. Plant Cell 24 2105-2122
808 Lo Presti, L., and Kahmann, R. 2017. How filamentous plant pathogen effectors are translocated
809 to host cells. Curr. Opin. Plant Biol. 38:19-24.
810 Lo Presti, L., Zechmann, B., Kumlehn, J., Liang, L., Lanver, D., Tanaka, S., Bock, R., and
811 Kahmann, R. 2017. An assay for entry of secreted fungal effectors into plant cells. New
812 Phytol. 213:956-964.
813 Lo Presti, L., Lanver, D., Schweizer, G., Tanaka, S., Liang, L., Tollot, M., Zuccaro, A., Reissmann,
814 S., and Kahmann, R. 2015. Fungal effectors and plant susceptibility. Annual Review of Plant
815 Biology 66:513-545.
816 Ludwig, N., Reissmann, S., Schipper, K., Gonzalez, C., Assmann, D., Glatter, T., Moretti, M., Ma,
817 L.-S., Rexer, K.-H., Snetselaar, K., and Kahmann, R. 2021. A cell surface-exposed protein
818 complex with an essential virulence function in *Ustilago maydis*. Nature Microbiology
819 6:722-730.
820 Manning, V.A., and Ciuffetti, L.M. 2005. Localization of Ptr ToxA produced by *Pyrenophora*
821 *tritici-repentis* reveals protein import into wheat mesophyll cells. Plant Cell 17:3203-3212.

822 Maranda, B., Brown, D., Bourgoin, S., Casanova, J.E., Vinay, P., Ausiello, D.A., and Marshansky,
823 V. 2001. Intra-endosomal pH-sensitive recruitment of the Arf-nucleotide exchange factor
824 ARNO and Arf6 from cytoplasm to proximal tubule endosomes. Journal of Biological
825 Chemistry 276:18540-18550.
826 Mbengue, M., Bourdais, G., Gervasi, F., Beck, M., Zhou, J., Spallek, T., Bartels, S., Boller, T.,
827 Ueda, T., Kuhn, H., and Robatzek, S. 2016. Clathrin-dependent endocytosis is required for
828 immunity mediated by pattern recognition receptor kinases. Proceedings of the National
829 Academy of Sciences 113:11034-11039.
830 Mentlak, T.A., Kombrink, A., Shinya, T., Ryder, L.S., Otomo, I., Saitoh, H., Terauchi, R.,
831 Nishizawa, Y., Shibuya, N., Thomma, B.P., and Talbot, N.J. 2012. Effector-mediated
832 suppression of chitin-triggered immunity by *Magnaporthe oryzae* is necessary for rice blast
833 disease. Plant Cell 24:322-335.
834 Mochizuki, S., Minami, E., and Nishizawa, Y. 2015. Live-cell imaging of rice cytological changes
835 reveals the importance of host vacuole maintenance for biotrophic invasion by blast fungus,
836 *Magnaporthe oryzae*. MicrobiologyOpen 4:952-966.
837 Mosquera, G., Giraldo, M.C., Khang, C.H., Coughlan, S., and Valent, B. 2009. Interaction
838 transcriptome analysis identifies *Magnaporthe oryzae* BAS1-4 as biotrophy-associated
839 secreted proteins in rice blast disease. Plant Cell 21:1273-1290.
840 Narasimhan, M., Johnson, A., Prizak, R., Kaufmann, W.A., Tan, S., Casillas-Pérez, B., and Friml,
841 J. 2020. Evolutionarily unique mechanistic framework of clathrin-mediated endocytosis in
842 plants. eLife 9:e52067.
843 Nishimura, T., Mochizuki, S., Ishii-Minami, N., Fujisawa, Y., Kawahara, Y., Yoshida, Y., Okada,
844 K., Ando, S., Matsumura, H., Terauchi, R., Minami, E., and Nishizawa, Y. 2016.
845 *Magnaporthe oryzae* glycine-rich secretion protein, Rbf1 critically participates in
846 pathogenicity through the focal formation of the biotrophic interfacial complex. PLoS Path.
847 12:e1005921.
848 Nishizawa, Y., Mochizuki, S., Yokotani, N., Nishimura, T., and Minami, E. 2016. Molecular and
849 cellular analysis of the biotrophic interaction between rice and *Magnaporthe oryzae* –
850 Exploring situations in which the blast fungus controls the infection. Physiol. Mol. Plant
851 Pathol. 95:70-76.

852 O'Connell, R.J., and Panstruga, R. 2006. Tête à tête inside a plant cell: establishing compatibility
853 between plants and biotrophic fungi and oomycetes. New Phytol. 171:699-718.
854 Otto, G.P., and Nichols, B.J. 2011. The roles of flotillin microdomains – endocytosis and beyond.
855 Journal of Cell Science 124:3933-3940.
856 Park, S.H., Park, J., and Smith, R.H. 2001. Herbicide and insect resistant elite transgenic rice.
857 Journal of Plant Physiology 158:1221-1226.
858 Petre, B., and Kamoun, S. 2014. How do filamentous pathogens deliver effector proteins into plant
859 cells? PLoS. Biol. 12:e1001801.
860 Petre, B., Contreras, M.P., Bozkurt, T.O., Schattat, M.H., Sklenar, J., Schornack, S., Abd-El-
861 Haliem, A., Castells-Graells, R., Lozano-Durán, R., Dagdas, Y.F., Menke, F.L.H., Jones,
862 A.M.E., Vossen, J.H., Robatzek, S., Kamoun, S., and Win, J. 2021. Host-interactor screens
863 of *Phytophthora infestans* RXLR proteins reveal vesicle trafficking as a major effector-
864 targeted process. Plant Cell 33:1447-1471.
865 Postma, J., Liebrand, T.W.H., Bi, G., Evrard, A., Bye, R.R., Mbengue, M., Kuhn, H., Joosten,
866 M.H.A.J., and Robatzek, S. 2016. Avr4 promotes Cf-4 receptor-like protein association with
867 the BAK1/SERK3 receptor-like kinase to initiate receptor endocytosis and plant immunity.
868 New Phytol. 210:627-642.
869 Qi, X., Pleskot, R., Irani, N.G., and Van Damme, D. 2018. Meeting report – Cellular gateways:
870 expanding the role of endocytosis in plant development. Journal of Cell Science
871 131:jcs222604.
872 Reynolds, G.D., Wang, C., Pan, J., and Bednarek, S.Y. 2018. Inroads into internalization: Five
873 years of endocytic exploration. Plant Physiology 176:208-218.
874 Robinson, D.G., Jiang, L.W., and Schumacher, K. 2008. The endosomal system of plants: Charting
875 new and familiar territories. Plant Physiology 147:1482-1492.
876 Rodal, S.K., Skretting, G., Garred, O., Vilhardt, F., van Deurs, B., and Sandvig, K. 1999.
877 Extraction of cholesterol with methyl-beta-cyclodextrin perturbs formation of clathrin-
878 coated endocytic vesicles. Molecular Biology of the Cell 10:961-974.
879 Sachse, M., Urbe, S., Oorschot, V., Strous, G.J., and Klumperman, J. 2002. Bilayered clathrin
880 coats on endosomal vacuoles are involved in protein sorting toward lysosomes Molecular
881 Biology of the Cell 13:1313-1328

882 Sakulkoo, W., Oses-Ruiz, M., Garcia, E.O., Soanes, D.M., Littlejohn, G.R., Hacker, C., Correia,
883 A., Valent, B., and Talbot, N.J. 2018. A single fungal MAP kinase controls plant cell-to-cell
884 invasion by the rice blast fungus. Science 359:1399-1403.
885 Serrano, M., Robatzek, S., Torres, M., Kombrink, E., Somssich, I.E., Robinson, M., and Schulze-
886 Lefert, P. 2007. Chemical interference of pathogen-associated molecular pattern-triggered
887 immune responses in Arabidopsis reveals a potential role for fatty-acid synthase type II
888 complexderived lipid signals. Journal of Biological Chemistry 282:6803-6811.
889 Spallek, T., Beck, M., Ben Khaled, S., Salomon, S., Bourdais, G., Schellmann, S., and Robatzek,
890 S. 2013. ESCRT-I mediates FLS2 endosomal sorting and plant immunity. PLoS Genetics
891 9:e1004035.
892 Stark-Urnau, M., and Mendgen, K. 1995. Sequential deposition of plant glycoproteins and
893 polysaccharides at the host-parasite interface of *Uromyces vignae* and *Vigna sinensis*:
894 Evidence for endocytosis and secretion. Protoplasma 186:1-11.
895 Sweigard, J. A., Carroll, A. M., Kang, S., Farrall, L., Chumley, F. G., and Valent, B. 1995.
896 Identification, cloning, and characterization of *PWL2*, a gene for host species specificity in
897 the rice blast fungus. Plant Cell 7:1221-1233.
898 Trusch, F., Loebach, L., Wawra, S., Durward, E., Wuensch, A., Iberahim, N.A., de Bruijn, I.,
899 MacKenzie, K., Willems, A., Toloczko, A., Diéguez-Uribeondo, J., Rasmussen, T.,
900 Schrader, T., Bayer, P., Secombes, C.J., and van West, P. 2018. Cell entry of a host-targeting
901 protein of oomycetes requires gp96. Nat. Comm. 9:2347.
902 Valent, B., and Chumley, F.G. 1991. Molecular genetic analysis of the rice blast fungus,
903 *Magnaporthe grisea*. Annu. Rev. Phytopathol. 29:443-467.
904 Valent, B., Singh, P.K., He, X., Farman, M., Tosa, Y., and Braun, H.J. 2020. Blast diseases:
905 Evolution and challenges of a staple food crop fungal pathogen. Pages 267-292 in: Emerging
906 Plant Diseases and Global Food Security, J.B. Ristaino and A. Records, eds. American
907 Phytopathological Society Press, St. Paul, MN.
908 Van den Ackerveken, G. 2017. Seeing is believing: imaging the delivery of pathogen effectors
909 during plant infection. New Phytol. 216:8-10.
910 Wang, L.H., Rothberg, K.G., and Anderson, R.G. 1993. Misassembly of clathrin lattices on
911 endosomes reveals a regulatory switch for coated pit formation Journal of Cell Biology
912 123:1107-1117.

913 Wang, S., Boevink, P.C., Welsh, L., Zhang, R., Whisson, S.C., and Birch, P.R.J. 2017. Delivery
914 of cytoplasmic and apoplastic effectors from *Phytophthora infestans* haustoria by distinct
915 secretion pathways. New Phytol. 216:205-215.
916 Wawra, S., Trusch, F., Matena, A., Apostolakis, K., Linne, U., Zhukov, I., Stanek, J., Koźmiński,
917 W., Davidson, I., Secombes, C.J., Bayer, P., and van West, P. 2017. The RxLR motif of the
918 host targeting effector AVR3a of *Phytophthora infestans* is cleaved before secretion. Plant
919 Cell 29:1184-1195.
920 Xu, J.-R., Staiger, C.J., and Hamer, J.E. 1998. Inactivation of the mitogen-activated protein
921 kinase Mps1 from the rice blast fungus prevents penetration of host cells but allows
922 activation of plant defense responses. Proceedings of the National Academy of Sciences
923 U.S.A. 95:12713-12718

924 **Table 1. Chemical inhibitors of endocytosis**

Chemical	Target	Mode of action	Comments	References
Filipin	CIE*	Binds to sterols in the membrane.	Toxic at higher concentrations.	(Rodal et al., 1999)
Methyl-β-cyclodextrin	CIE	Deplete cellular membranes of sterols by increasing the water solubility of the sterol.	caveolae-dependent endocytosis.	(Rodal et al., 1999)
Chlorpromazine	CME**	Translocates clathrin and AP2 from the cell surface to intracellular endosomes.	Also inhibits CIE in some cells.	(Wang et al., 1993)
Cantharidin	CME	Inhibits PP2A (protein phosphatase 2A)	Affects flg22-mediated FLS2 endocytosis.	(Serrano et al., 2007)
Triclosan	CME	Inhibits PP2A (protein phosphatase 2A)	Affects flg22-mediated FLS2 endocytosis.	(Serrano et al., 2007)
Wortmannin	nd***	Inhibits PI3Ks, blocks late trafficking to the vacuole, multivesicular bodies and endocytosis.	Late endosomes lose their clathrin; Potential CME association.	(Bright et al., 2001; Sachse et al., 2002; Robinson et al., 2008)
Concanamycin A	nd	Targets V-type ATPase and blocks trafficking at trans-Golgi network, endosome acidification.	Induces acidification crucial for endocytic pathways.	(Maranda et al., 2001; Robinson et al., 2008)

925 *CIE: clathrin-independent endocytosis; **CME: clathrin-mediated endocytosis; ***nd: not determined.

926

927 Figure 1

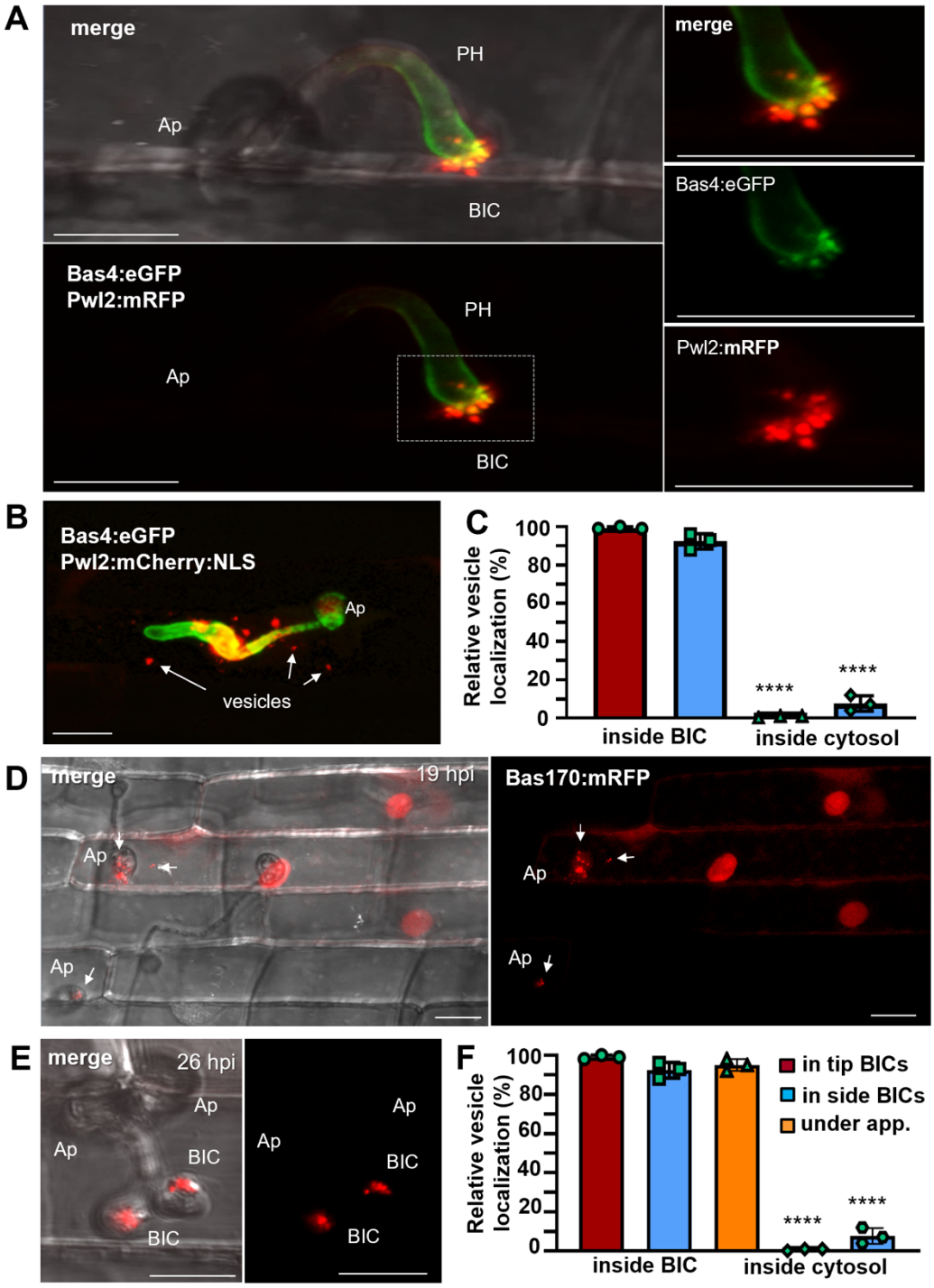

928

929 **Figure 1**. **BIC vesicular organization and effector vesicles in the rice cell cytoplasm**. **A.**
930 Cytoplasmic effector-labeled vesicles in a tip-BIC at the tip of a primary hypha (PH) of strain
931 KV217 expressing Pwl2:mRFP and Bas4:eGFP at 17 hpi. The appressorium (Ap) and the first half
932 of the PH are out of focus. Separate mRFP and eGFP channels (right) for the inset show the base
933 layer of apoplastic effector Bas4:eGFP and the outer vesicular layer labeled by cytoplasmic

934 effector Pwl2:mRFP. **B.** A side-BIC occurring above a first bulbous IH cell of strain KV168
935 expressing Pwl2:mCherry:NLS and Bas4:eGFP at 24 hpi. Effector vesicles in are visible in the
936 host cytoplasm at a distance from the BIC. The Bas4:eGFP control shows that the EIHM
937 surrounding the IH remains intact. See Supplemental Figure S2 for a larger view of this invaded
938 cell showing significant host translocation of Pwl2:mCherry:NLS. **C.** Quantification of the relative
939 localization of cytoplasmic effector vesicles, assessed using strain KV217 from panel A at 98
940 infection sites for each BIC developmental stage. Bar charts are based on means of three biological
941 reps (data points shown); error bars indicate standard deviation. ****P<0.0001. **D.** Bas170:mRFP,
942 here expressed by *M. oryzae* strain KV224, shows rapid accumulation in vesicles under appressoria
943 and in plant nuclei. At 19 hpi, Bas170:mRFP labels vesicles under appressoria and naturally
944 accumulates in nuclei even before a primary hypha is visible. Arrows indicate vesicles in the rice
945 cytoplasm. Left image shows merged bright field and mRFP fluorescence and right image shows
946 mRFP fluorescence alone. **E.** Bas170:mRFP also localizes to BICs, shown here at 26 hpi in side-
947 BICs resulting from adjacent appressoria penetrating the same rice cell. Experimental details same
948 as in D. **F.** Quantification of the relative localizations of Bas170:mRFP effector vesicles, assessed
949 using data from strain KV224 (D and E) at 98 infection sites for each BIC developmental stage
950 and cytoplasm under appressoria (app.) during fungal penetration. Bar charts with data points from
951 biological replications same as described in C. All images are projections of confocal optical
952 sections. Images in A and B (merged bright field, eGFP and mRFP fluorescence) shown as
953 projections of confocal optical sections. Bars = 10 µm.
954

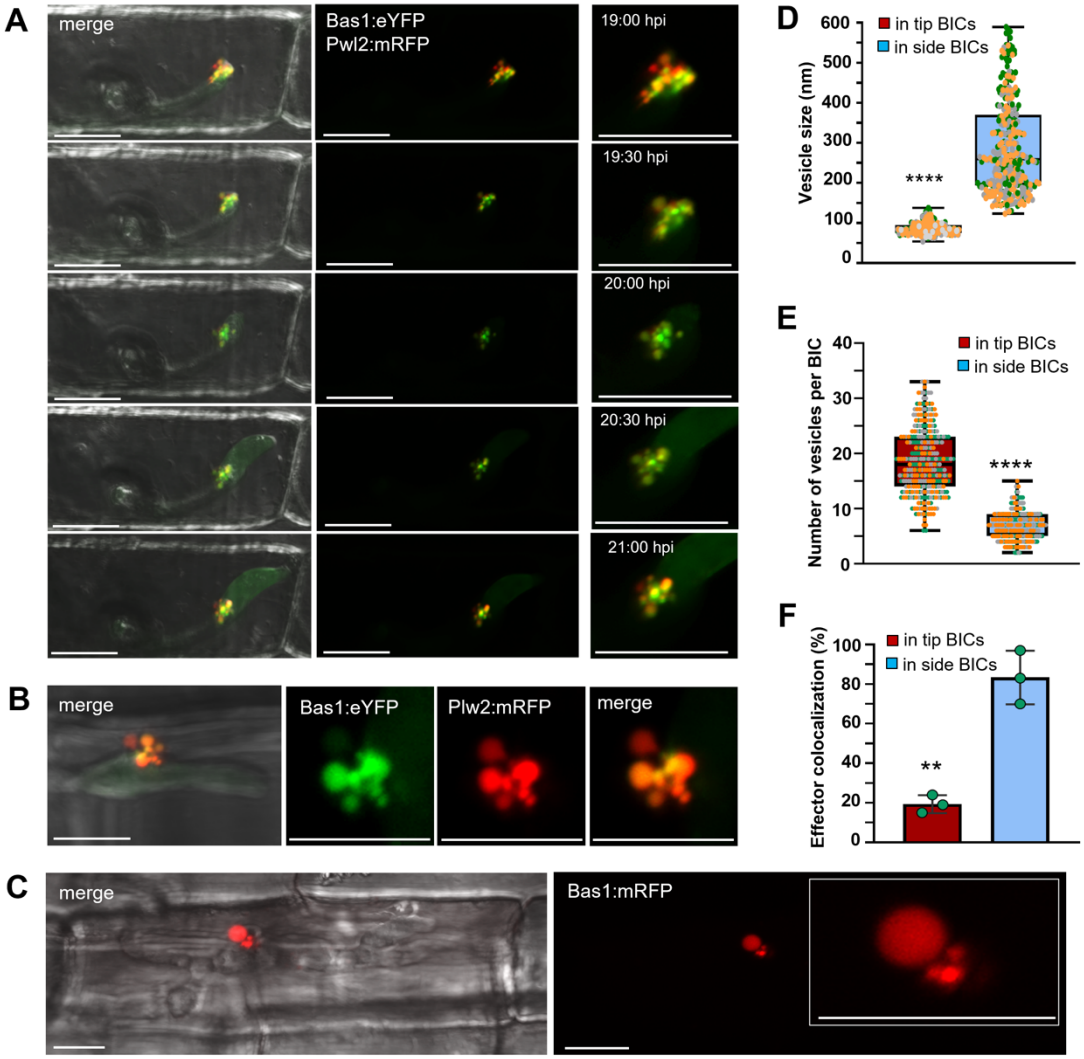

Figure 2. Dynamics of BICs and effector vesicles during differentiation of primary hyphae to first bulbous invasive hyphae. A. Dynamics of two cytoplasmic effectors, Pwl2:mRFP and Bas1:eYFP (Strain KV211), as a tip-BIC (top panel) becomes a side-BIC (bottom panel), imaged every 30 min from 19 to 21 hpi. Images (left to right) are merged bright field, eYFP and mRFP fluorescence at 5 time points; merged eYFP and mRFP at same time points in both the same and enlarged views of the fluorescent BICs shown as projections of confocal optical sections. Bars = 10 µm. **B.** Cytoplasmic effectors Pwl2:mRFP and Bas1:eYFP (Strain KV211) co-localize in larger vesicles in a side-BIC at 24 hpi. **C.** A rare extremely large effector vesicle (diameter 3.9 µm) in a late stage side-BIC formed by strain KV170 expressing Bas1:mRFP at 30 hpi. **D,E.** Box and whisker plots with individual data points comparing vesicle sizes (D) and number of vesicles (E) in tip- and side-BICs formed by strain KV211 invading rice cells; data points of different colors represent different biological replicates. **F.** Bar chart showing quantification of Bas1:eYFP and Pwl2:mRFP colocalization (KV211) in vesicles in tip- and side-BICs. Bar charts are based on mean values of data points from three biological replicates; error bars indicate standard deviation. **P=0.0015; ****P<0.0001. 100 BICs observed per replicate in D-F.

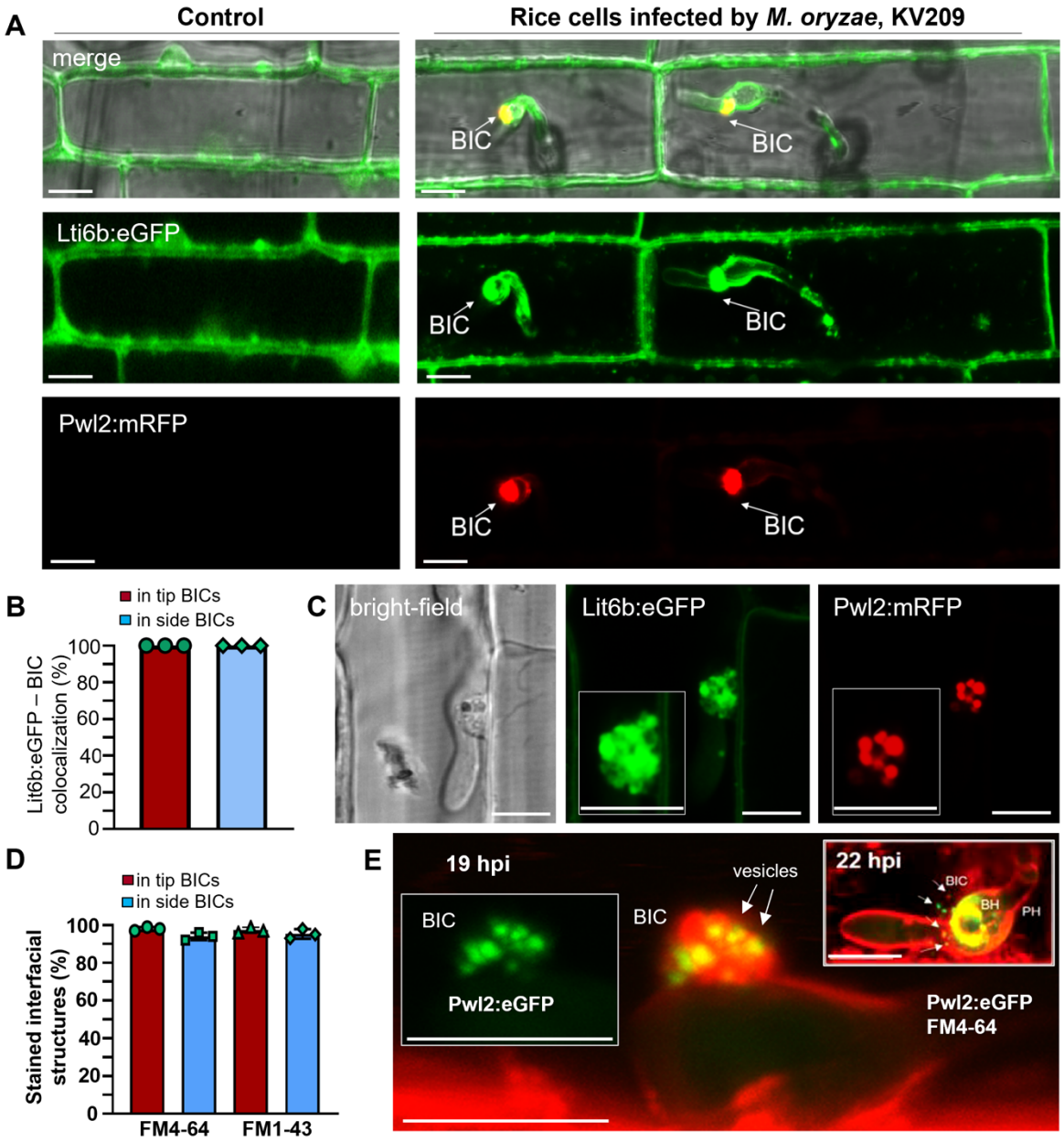

Figure 3. Effector vesicles are derived from plant plasma membrane. A. Rice expressing plasma membrane marker LTi6b:eGFP in non-infected cells (left column) and in cells infected by strain KV209 expressing Pwl2:mRFP (right column). Colocalization confirms BICs as plant plasma membrane-rich structures. **B.** Quantification of the colocalization of LTi6b:eGFP with BICs at both developmental stages. Bar charts are based on means of three biological reps (data points shown); error bars indicate standard deviation; three times 90 infection sites observed. **C.** Localization assays of LTi6b:eGFP relative to Pwl2:mRFP in an infected rice cell at 22 hpi showing LTi6b:eGFP outlining vesicles in the BIC. Insets show BIC vesicles at higher magnification. **D.** Quantification of BICs stained by the endocytosis tracer dyes FM 4-64 and FM 1-43 at the tips of primary hyphae and beside the first bulbous IH. Bar charts are based on means of three biological reps (data points shown); error bars indicate standard deviation; three times 90

983 infection sites observed per treatment. **E.** Colocalization of BIC effector vesicles and FM4-64-
984 stained membranes in BICs. The main image shows strain KV176 expressing Pwl2:eGFP in a side-
985 BIC in FM 4-64 stained rice at 19 hpi. The image shows merged eGFP and FM 4-64 fluorescence
986 with eGFP fluorescence shown alone in the inset in the lower left. The upper right inset shows a
987 top-down view of a different BIC, shown below the image plane, at 22 hpi. Inset arrows indicate
988 Pwl2:eGFP vesicles near the BIC. Images are projections of confocal optical sections. See
989 Supplemental Movie S2 for yet another side-BIC with additional examples of colocalization of
990 FM 4-64 fluorescence and Pwl2:eGFP. All Bars = 10 µm.

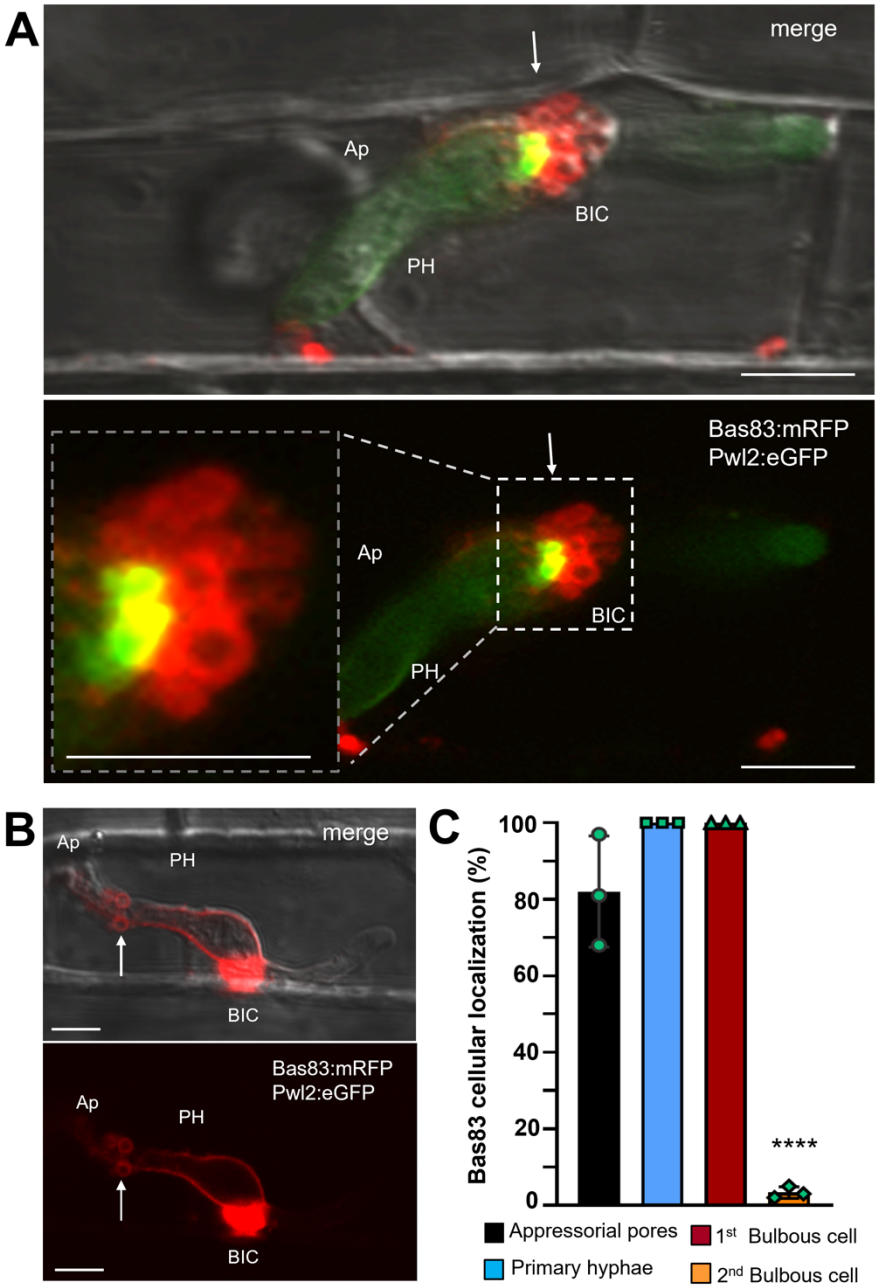

Figure 4. Bas83 is a novel effector associated membrane vesicles surrounding BICs and BIC-associated cells. A. Bas83:mRFP binds apparent membrane vesicles surrounding a side-BIC (white arrow) labeled with Pwl2:eGFP (strain KV222). **B.** Bas83:mRFP (KV220) binds to bubble-like structures near a primary hypha (arrow) as well as labeling a BIC and outlining BIC-associated cells. Images (merged bright field, eGFP and mRFP fluorescence) are projections of confocal optical sections. See additional images in Supplemental Figure S3. Bars = 10 µm. **C.** Quantification of the cellular localization of Bas83:mRFP during biotrophic invasion of *M. oryzae* (KV220). Bar charts are based on means of three biological reps (data points shown); error bars indicate standard deviation. ****P<0.0001; 100 infection sites observed per experiment.

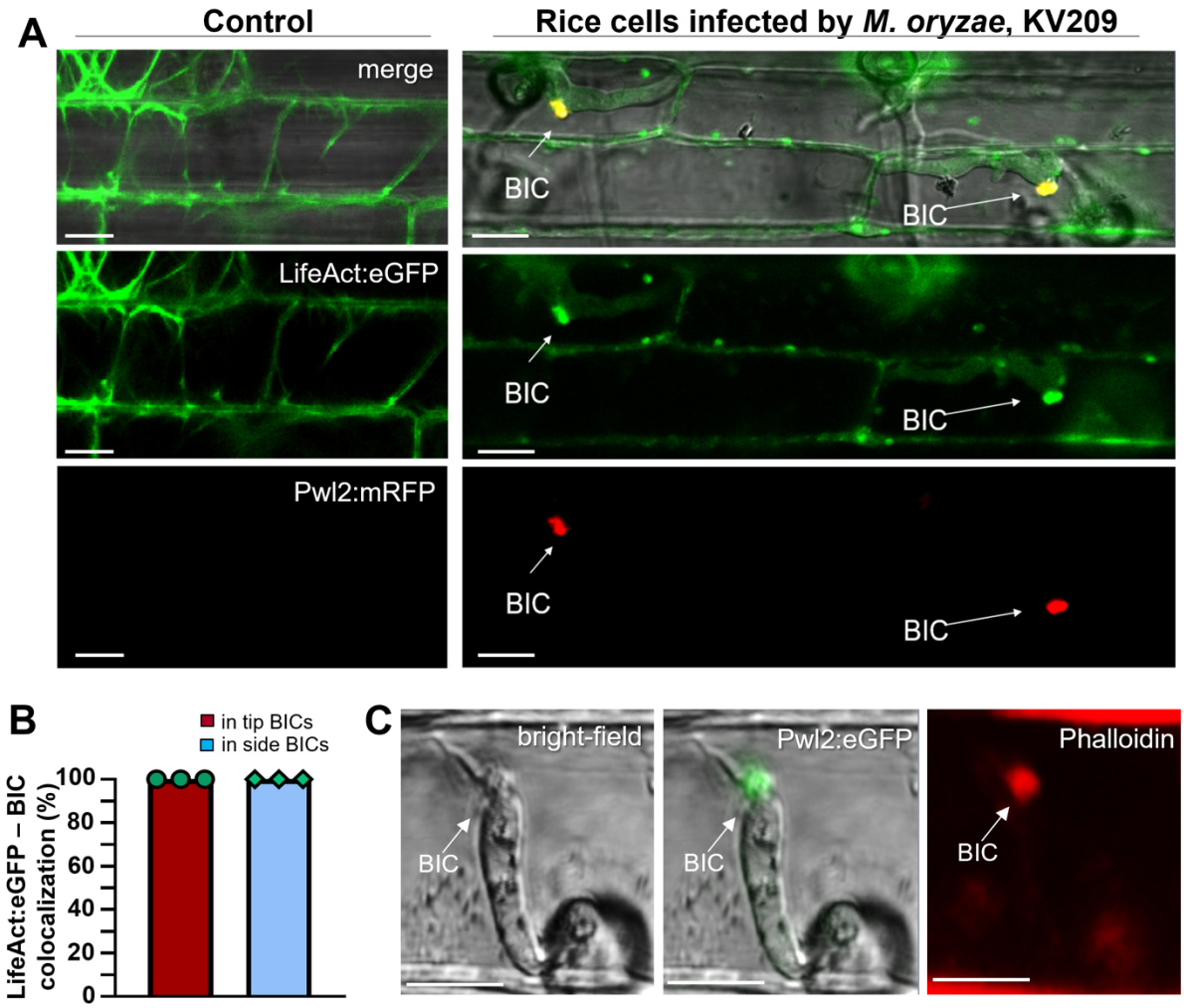

Figure 5. BICs contain plant actin. A. Rice LifeAct:eGFP localization during biotrophic invasion by *M. oryzae*. A rice line expressing LifeAct:eGFP in non-infected cells (left column) and cells infected by *M. oryzae* strain KV209 expressing Pwl2:mRFP in BICs (right column). Colocalization shows BICs are rich in plant actin. **B.** Quantification of the colocalization of LifeAct:eGFP with both tip- and side-BICs. Bar charts are based on means of three biological reps (data points shown); error bars indicate standard deviation; three times 100 infection sites observed. **C.** Rhodamine phalloidin conjugate (red fluorescence staining actin filaments) colocalizes with Pwl2:eGFP in rice cells infected by strain KV176, confirming the actin-rich structure of the BIC.

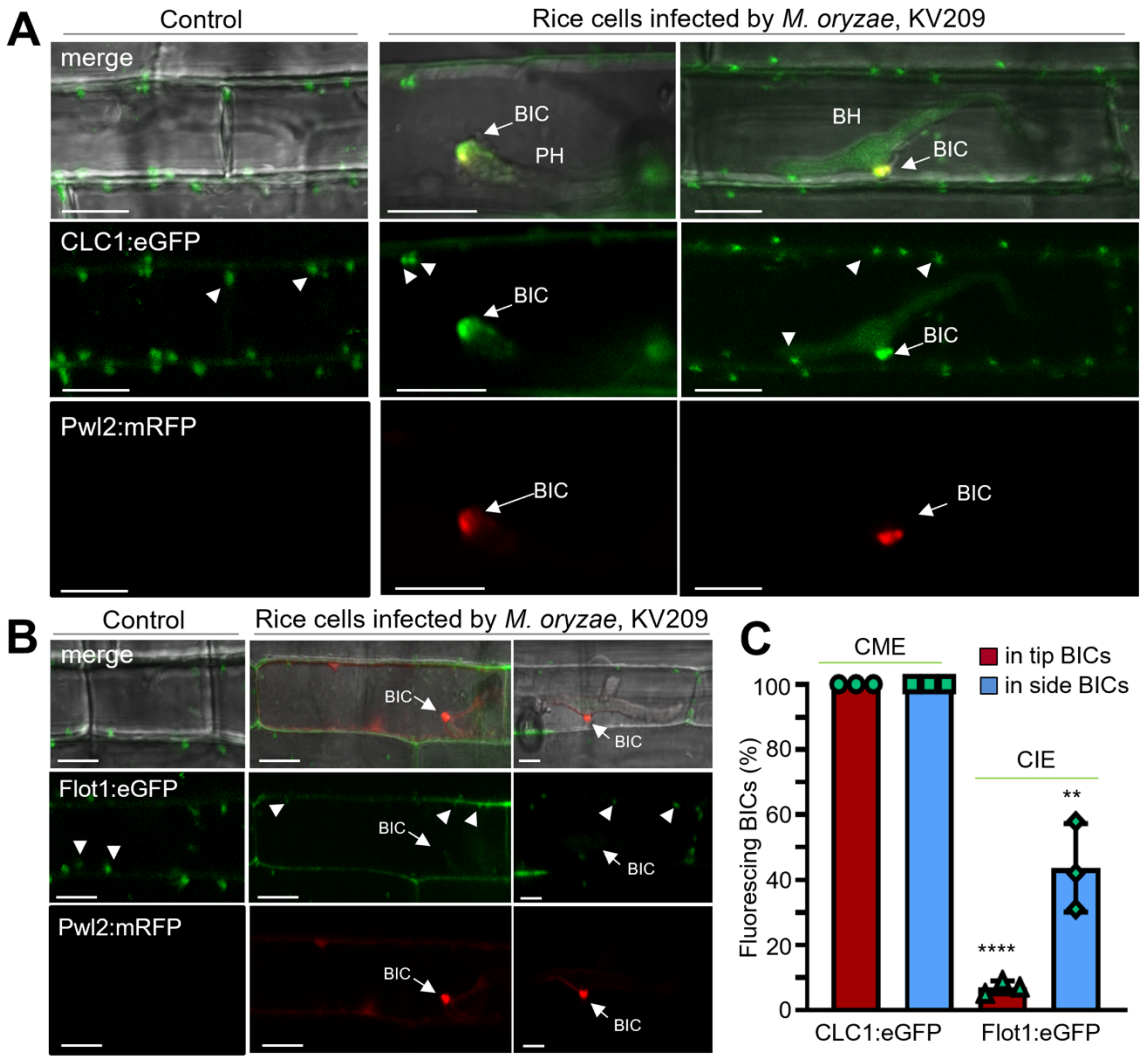

Figure 6. BICs uniformly contain clathrin, but not in flotillin1. A. Rice leaf sheaths expressing OsCLC1:eGFP (CME marker) were inoculated with strain KV209 expressing Pwl2:mRFP. Shown from left to right are a non-infected rice sheath cell; an infected cell containing a primary hypha (PH) with a tip-BIC at 19 hpi; and an infected cell containing a bulbous IH (BH) with a side-BIC at 22 hpi. Arrowheads indicate endocytic foci and arrows indicate BICs. Bars=10µm. **B.** Rice leaf sheaths expressing OsFlot1:eGFP (CIE marker) were inoculated with KV209 expressing Pwl2:mRFP, as in panel A. Shown from left to right are a non-infected rice sheath cell; an infected cell containing a primary hypha with a tip-BIC at 19 hpi; and an infected cell containing a bulbous IH with a side-BIC at 22 hpi. Arrowheads indicate endocytic foci and arrows indicate BICs. Bars=10µm. **C.** Quantification of the colocalization of OsCLC1:eGFP or OsFlot1:eGFP in both BIC developmental stages. Bar charts are based on means of three biological reps (data points shown); error bars indicate standard deviation; three times 97 BICs observed each treatment. ****P<0.0001; **P=0.002. CME, clathrin-mediated endocytosis; CIE, clathrin-independent endocytosis.

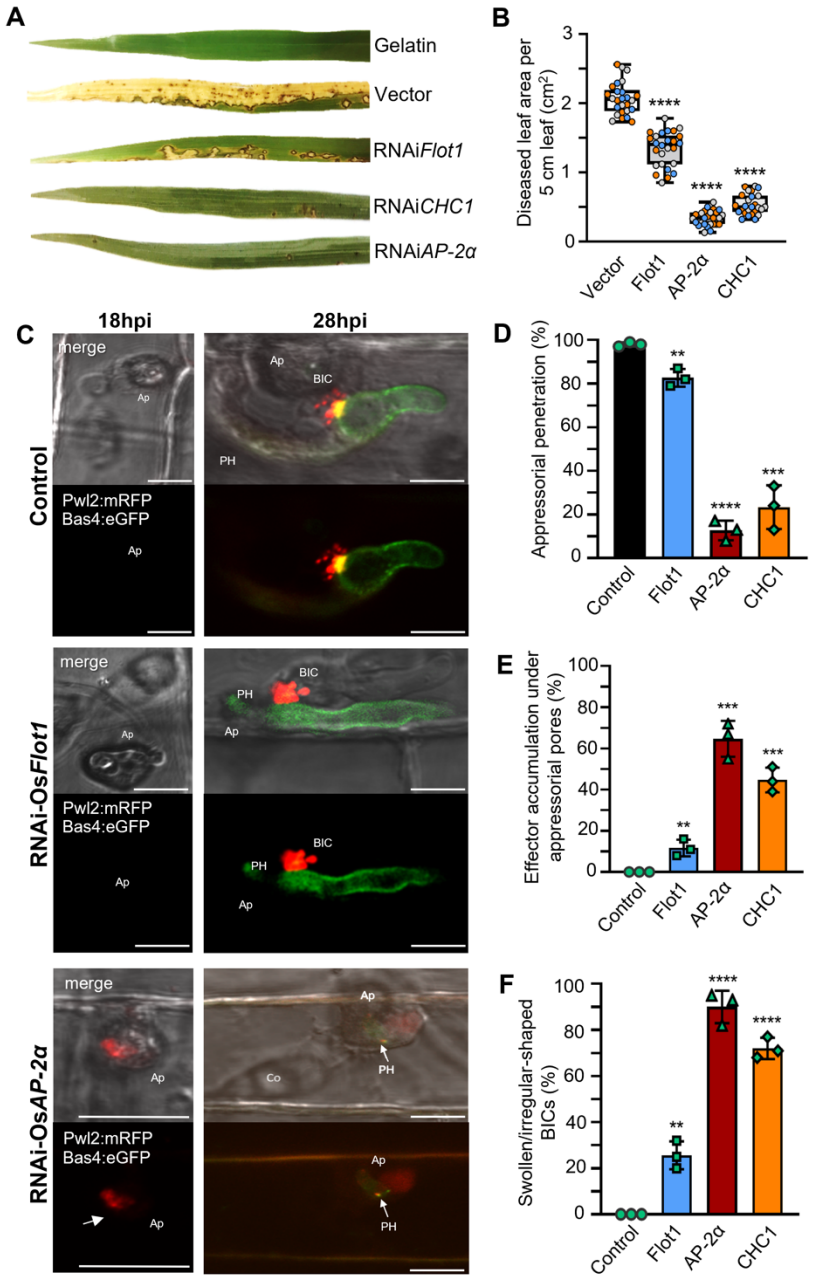

Figure 7. Silencing of rice endocytic machinery suggests roles in pathogenicity and fungal effector translocation. A. Disease severity in rice leaves, cultivar IR64, undergoing silencing of rice endocytic genes**.** Whereas silencing of *Flot1* gene showed minor effects on pathogenesis, the silencing of the key clathrin-mediated endocytosis genes, *AP-2α* and CHC1 resulted in a significant reduction in pathogenicity in whole plant spray inoculation assays. **B.** Quantification of diseased area in 5cm leaf segments in rice expressing RNAi*AP-2α*, RNAi*CHC1*, RNAi*Flot1* or empty vector infected by *M. oryzae* strain Guy11. Box and whisker plots with individual data points are shown; data points of different colors represent different biological replicates. ($P<0.0001$ for all treatments; n = 9 rice plants per replication). **C.** Effects of silencing rice endocytosis genes on the localization of Pwl2:mRFP and Bas4:eGFP during biotrophic invasion.

1039 Wild type IR64 rice and rice expressing RNAi*Flot1* or RNAi*AP-2*α were infected by KV217
1040 expressing Pwl2:mRFP and Bas4:eGFP at 26 hpi. Note the accumulation of Pwl2:mRFP under the
1041 appressorium (Ap) and the pale Bas4:eGFP fluorescence associated with the short primary hypha
1042 (PH) in the RNAi*AP2*α rice compared to the control and RNAi*Flot1* rice. Images in C (merged
1043 bright field, eGFP and mRFP fluorescence) are shown as projections of confocal optical sections.
1044 Bars = 10 µm. **D.-F.** Quantification of appressorial penetration (D), effector accumulation under
1045 appressoria (E), and swollen irregular BICs (F) in rice expressing RNAi*Flot1*, RNAi*AP-2*α,
1046 RNAi*CHC1* or the empty vector during infection by strain KV209 expressing Pwl2:mRFP (~28
1047 hpi). Bar charts are based on means of three biological reps (data points shown); error bars indicate
1048 standard deviation. (D: **P=0.0031, ***P=0.0002, ****P<0.0001; E: **P=0.0075, ***P=0.0002;
1049 F: **P=0.0018, ****<0.0001; three times 100 infection sites counted per treatment).
1050

1051 Figure 8

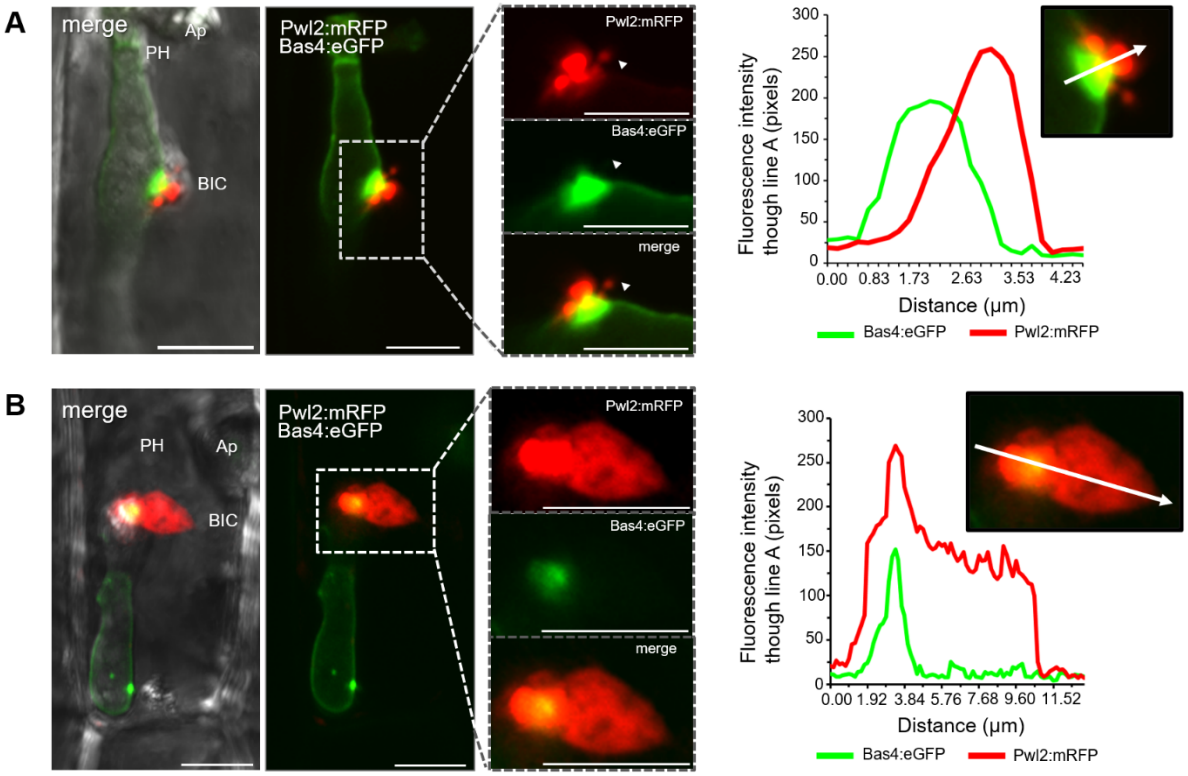

1052
1053 **Figure 8. Treatment with CME inhibitor cantharidin impacts the localization of cytoplasmic**
1054 **effector Pwl2, but not apoplastic effector Bas4. A.** Apoplastic effector Bas4:eGFP identifies an
1055 inner base layer of the BIC relative to cytoplasmic Pwl2:mRFP, as shown by fluorescence intensity
1056 linescans for GFP (green) and mRFP (red) along the path of the white arrow. This side-BIC was
1057 formed during invasion of rice by strain KV217 expressing Pwl2:mRFP and Bas4:eGFP at 26 hpi.
1058 **B.** After treatment with CME inhibitor cantharidin, localization of Bas4:eGFP in the BIC base
1059 appears unaffected, compared to the non-vesicular swollen localization of Pwl2:mRFP, as shown
1060 by fluorescence intensity linescans for GFP (green) and mRFP (red) along the path of the white
1061 arrow. Note linescan distance for Pwl2:mRFP is almost 3-fold greater after cantharidin treatment.
1062 This BIC was formed by KV217 at 26 hpi, as in control panel A. Images (merged bright field,
1063 eGFP and mRFP fluorescence) are shown as projections of confocal optical sections.
1064 Appressorium (Ap); Primary hypha (PH). Bars = 10 µm.
1065

1066 Figure 9

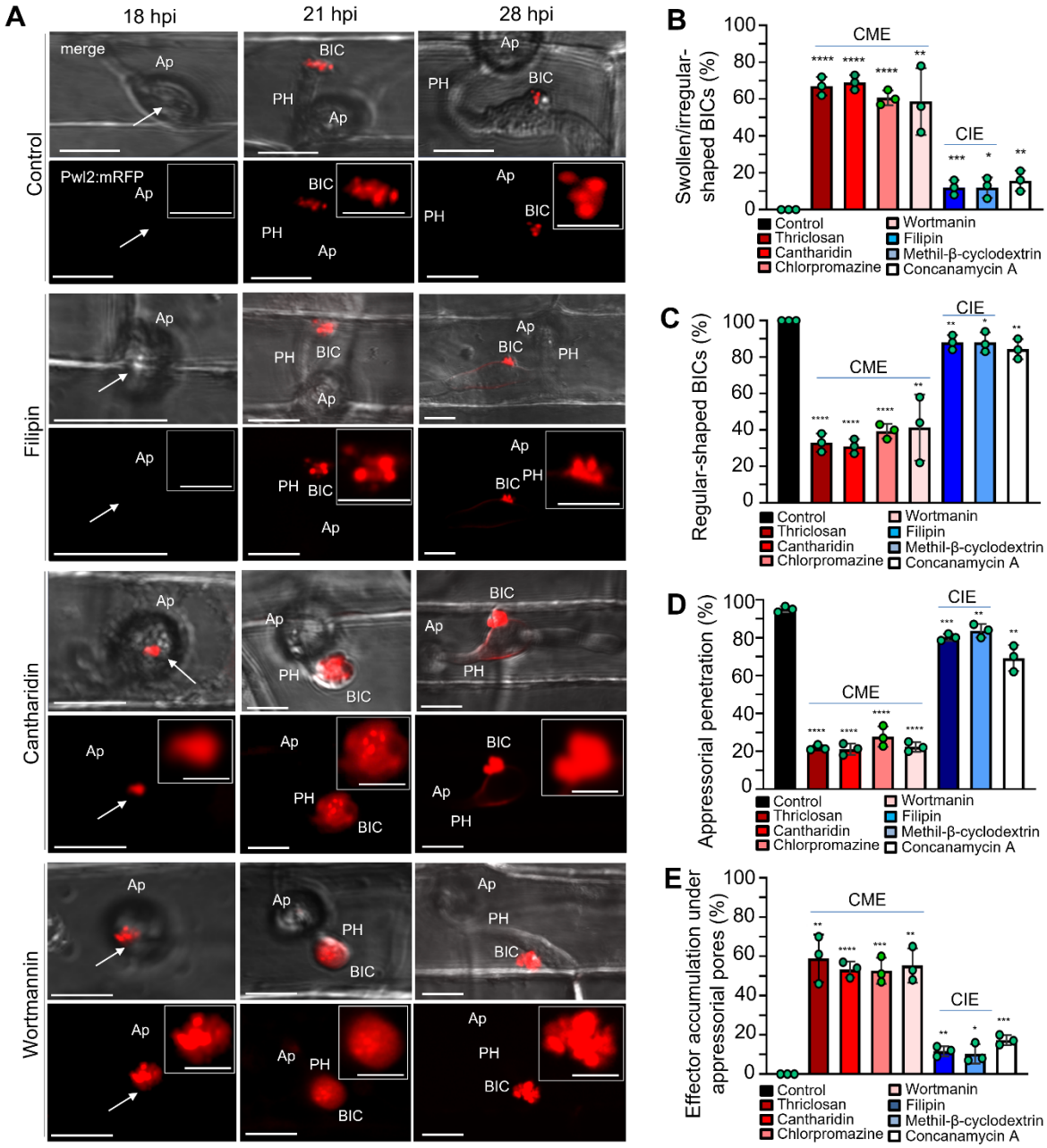

1067

1068 **Figure 9. Chemical inhibition of rice CME, but not of CIE, has a major impact on**
1069 **cytoplasmic effector localization and appressorial penetration. A.** Effects of chemical
1070 inhibition of Clathrin-mediated endocytosis (CME) and Clathrin-independent endocytosis (CIE)
1071 in the rice leaf sheath assay with strain KV209 expressing Pwl2:mRFP at 18, 21 and 28 hpi.
1072 Whereas inhibition of CIE showed significant, but relatively minor effects on BIC functionality
1073 and effector uptake, the chemical inhibition of CME resulted in a significant accumulation of
1074 effector fluorescence under appressoria (Ap, white arrows at 18 hpi) as well as swollen BICs on
1075 primary hyphae (PH, 21 hpi) and bulbous IH (28hpi). Images in A (merged bright field and mRFP
1076 fluorescence) are projections of confocal optical sections. Insets show close-up views of the

1077 effector fluorescence. Bars = 10 µm and bars in the insert boxes = 5 µm. **B-E.** Quantification of
1078 swollen, irregular-shaped BICs (B), regular-shaped BICs (C), appressorial penetration (D), and
1079 effector accumulation under appressoria (E), in rice undergoing chemical treatment and infection
1080 by strain KV209 expressing Pwl2:mRFP at 28 hpi. Bar charts are based on means of three
1081 biological reps (data points shown); error bars indicate standard deviation. Three times 100
1082 infection sites observed per treatment. B: *P=0.0202(MβC), **P=0.0065(Filipin), **P=0.0079
1083 (Con.A), **P=0.005(Wort.), ****P<0.0001; C: *P=0.02(MβC), **P=0.0065(Filipin),
1084 **P=0.0075(Con.A), **P=0.005(Wort.), ****P<0.0001; D: P=0.0068(MβC),
1085 **P=0.0004(Filipin), **P=0.0032 (Con.A), ****P<0.0001; E: *P=0.0222(MβC),
1086 **P=0.0013(Filipin), ***P=0.0003(Con.A), **P=0.0004(Wort.), **P=0.0011(Tricl.),
1087 ***P=0.0002(Chlorpr.), ****P<0.0001(Canth.).

1088 Figure 10

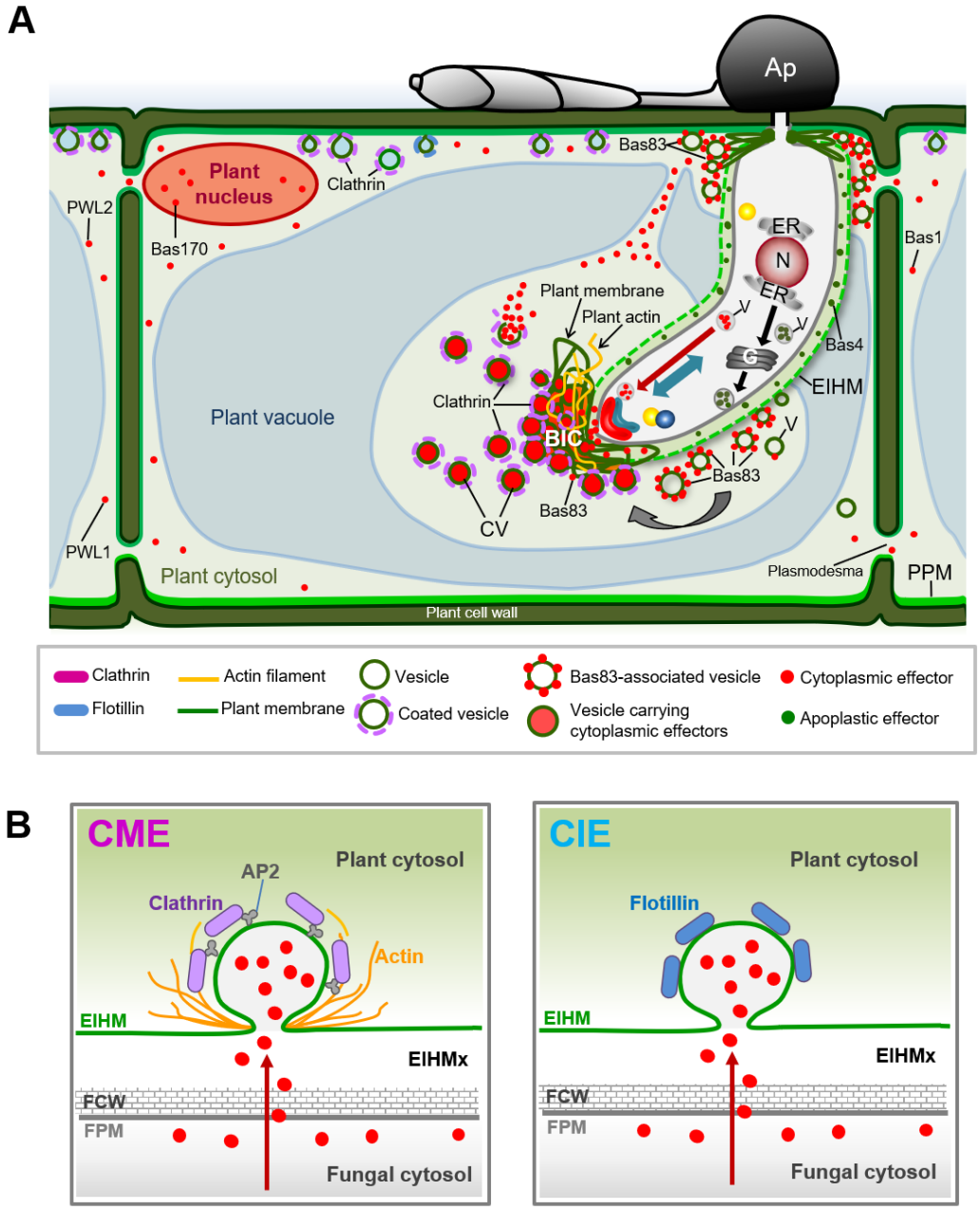

1089
1090 **Figure 10. Model for *M. oryzae* effector secretion and translocation into rice cells. A.** This
1091 cartoon represents the specialized Biotrophic Interfacial Complex at the growing tip of primary
1092 hyphae (tip-BIC) at 22–24 h.p.i. (hours post-inoculation), but similar mechanisms apply to side-
1093 BICs left behind after differentiation of the first bulbous invasive hyphae (IH). At successful
1094 infection sites, apoplastic effectors (dark green circles), including Biotrophy-associated secreted
1095 protein-4 (Bas4), are secreted from the PH by conventional golgi-dependent secretion (black
1096 arrows), which is blocked by treatment with Brefeldin A. Apoplastic effectors accumulate in the
1097 separate compartment enclosed by the EIHM (inside the dark green dashed line around the PH).
1098 In contrast, fluorescently-labeled cytoplasmic effectors (red circles), including Pwl2, Pwl1 and

1099 Bas1, are secreted into BICs by a nonconventional, Brefeldin A-insensitive secretion system
1100 involving the exocyst and SNARE protein Sso1 (red arrows). Cytoplasmic effectors also
1101 accumulate inside the EIHM compartment around the BIC-associated cells, the PH and first
1102 differentiated bulbous IH cell (not shown). In contrast, cytoplasmic effectors do not accumulate in
1103 the EIHM surrounding nonBIC-associated hyphal cells, which are tightly surrounded by the host
1104 vacuole. Our current study expands this model by showing that cytoplasmic effectors are packaged
1105 in dynamic vesicles inside BICs and they can sometimes be observed in the host cytoplasm
1106 surrounding BICs, and that these effector vesicles co-localize with fluorescent plant plasma
1107 membrane markers LTi6B:GFP and FM 4-64, as well as clathrin-mediated endocytosis (CME)
1108 marker CLC1:eGFP. These co-localization studies, additional localization with plant actin in BICs,
1109 and functional analyses via VIGS and pharmacological inhibitors support CME as a major
1110 mechanism for effector translocation. Further research should focus on two novel cytoplasmic
1111 effectors we describe. Bas83 labels empty membrane vesicles, possibly recruiting more host
1112 membrane to the BIC and the EIHM surrounding BIC-associated cells. Bas170 localizes to effector
1113 vesicles directly under the appressorium and accumulates in the host nucleus between BICs and
1114 the host cell periphery would facilitate movement of translocated effectors to the host nucleus and
1115 other sites of action in the host cell, as well as movement of cytoplasmic effectors through
1116 plasmodesmata into surrounding host cells to prepare them for invasion. Key: N, fungal nucleus;
1117 ER, endoplasmic reticulum; G, Golgi apparatus; V, transport vesicle. **B.** Working models for
1118 vesicle formation and effector translocation in the rice-*M. oryzae* interaction through CME or
1119 clathrin-independent endocytosis (CIE). Although our current work supports a role for CME, some
1120 involvement of CIE in effector translocation cannot be ruled out as playing a minor role. AP2,
1121 Adaptor Protein-2 complex; EIHM, extrainvasive hyphal membrane; EIHMx, extrainvasive
1122 hyphal matrix; FPM, fungal plasma membrane; FCW, fungal cell wall.